Assessment of Inter-Grid Transformation for Complete Aircraft Aeroelastic Analysis

Abdul Moosa Rampurawala

An Assessment of Inter-Grid Transformation for a Whole Aircraft

by

Abdul Moosa Rampurawala
B.E.[Aeronautics], University of Madras, Madras 2000

Thesis submitted to the Faculty of Engineering, in fulfillment of the requirements for the Master of Science degree by research at the University of Glasgow

University of Glasgow
Faculty of Engineering
Department of Aerospace Engineering

Abstract

As modern military aircraft become lighter, faster and more maneuverable, the consideration of aeroelastic effects during the design process can provide significant benefits. Computational aeroelasticity provides an attractive alternative to wind tunnel testing of flexible models in terms of accurately predicting and simulating the various linear and non-linear phenomena in a cost effective way.

Computational Structural Dynamic (CSD) and Computational Fluid Dynamic (CFD) codes have reached a level of development where they can accurately analyse the structural and fluid behaviour. Aeroelastic simulation of individual components of an aircraft is now commonly done but problems arise when simulating a whole aircraft configuration. This is because the CSD solver calculates the elastic response of the aircraft on a structural grid which usually does not coincide with the CFD surface grid and hence a scheme is required to transfer displacement and force values between the CSD and CFD grids. The various aerodynamic surface patches are driven by different structural components which may require different transformation methods. For example a fuselage, if modelled as a 1-dimensional beam, would require a different transformation technique than the wings which are modelled as 2-dimensional plates. To address this, a modified version of the Constant Volume Tetrahedron (CVT) transformation scheme is proposed for 1-dimensional structural grids. A tagging procedure is used where the fluid grid nodes are identified as being driven by 1 or 2-dimensional structural components and then the appropriate version of the transformation scheme is applied. The other difficulty is that the component interfaces in the fluid grid need to match up properly for the simulation to be successful. To overcome this a weighting method has been developed which

forces the grid points at the component interfaces of the fluid grid to match up correctly by averaging the transformation within a predefined hierarchy.

In the current work, this methodology has been demonstrated on a generic F16 aircraft configuration. The robustness of the transformation technique is evaluated by using a number of structural models to drive the fluid surface motions.

Acknowledgements

I would like to thank my supervisor Dr. Badcock for his able guidance and dedicated support towards the successful completion of this project. This work would not have been possible without his insight and experience in the field and his careful monitoring of the progress. I would also like thank Dr. Goura for familiarising me with the topic during the incipient stages of the work and for her help in setting up of the structural models. I thank Dr. Huang of National Research Council (Canada) for supplying the 2D CAD geometry of the Structural Dynamics Model of the generic F16 aircraft. I am greatly indebted to the Foreign and Common Wealth Office and the British Council for funding my studies here through the Chevening Award. Finally a special to thanks to Dr. Saxena and Dr. Manoj of the Computational and Theoretical Fluid Dynamics Division of National Aerospace Laboratories (Bangalore) for introducing me to CFD during my trainee days under them.

Contents

Chapter 1

Introduction

1.1 Flutter

A wing can often be seen to flex during flight. An aircraft must be a light-weight structure in contrast to civil and some mechanical structures. The weight restriction results in reduced stiffness when compared with structures made of steel and concrete. An aircraft wing is relatively flexible, and easily bends and twists under the influence of air loads. During normal flight operation the static air loads on the wing are usually less than its structural strength and hence not destructive. An exception to this is wing divergence where the elastic restoring force of the deformed wing is less than the aerodynamic load which occurs beyond a certain air speed called the divergent speed. If the wing begins to twist and bend in a periodic manner, under certain conditions the dynamic loads may begin feeding the elastic motion of the wing, causing its amplitude to grow, which in turn causes increased loads or fatigue, eventually causing structural failure. Such a catastrophic dynamic coupling between the elastic motion and the unsteady aerodynamic loading, causing synchronised vibrations, is called "flutter". A range of combinations of vibrations are possible. Each component of the aircraft has a natural (or fundamental) frequency. A classic case of wing flutter might combine wing bending with either wing

twisting (torsion) or the flapping of an aileron, which has the same lift-amplifying effect as twisting the wing. There are a number of other possibilities involving combinations of bending, twisting, and flapping, each with their own fundamental and harmonic frequencies, of wings, tails, fuselage, control surfaces, and trim tabs. An important type of flutter phenomenon, which has been observed in modern day fighter aircraft, is Limit Cycle Oscillation (LCO). The exact mechanism that leads to LCO is not yet properly understood and is a topic of research. It is suspected that it may be due to structural and aerodynamic nonlinearities like those in structural dynamics/kinametics, shock oscillations and shock induced flow separations [1]. LCO is characterised by a sustained periodic oscillation which neither increases nor decreases in time. Though not necessarily destructive it is a cause for decreased fatigue life and reduced precision of the weapon systems.

Flutter is mainly determined by stiffness and not by strength and hence even the strongest structure may fail due to flutter. In general, structures that are light and stiff vibrate more rapidly; i.e.they have higher natural frequencies. Structures more massive or less stiff have lower frequencies. Usually the flutter tendency of an aircraft is minimized by raising the natural frequency of one mode by stiffening it or by mass balance. The main objective of changing natural frequencies is to eliminate coincident frequencies that can exchange energy. A wing having non-similar torsional and flexural frequencies is less likely to flutter. Mass balancing is a widely practiced flutter prevention technique first studied and applied by von Baumhauer and Koning [2]. The basic idea is to increase the critical flutter speed by eliminating inertial coupling between the various components of the aircraft. This can be achieved by proper placement of components like engines and fuel tanks. It is essential to compute and analyse flutter to demonstrate the conditions of safe flight and to remove LCOs from the flight envelope.

Flutter has destroyed aircrafts since the early days of flying. A study was made by F.W. Lanchester during World War I for the Handley Page 0/400 biplane bomber

that experienced violent antisymmetric oscillations of the fuselage and the tail. It was found that the elevators moved independently as they were controlled by separate cables. The problem was solved by placing a torque tube between the elevators. A year after the report by Lanchester [3] a pilot fatality was caused in the de Havilland DH-9 aircraft [4]. The problem and the solution was identical to what Lanchester had earlier reported. In 1928 Frazer and Duncan published a detailed monograph on the flutter phenomenon [5] referred to as "The Flutter Bible" in Britain [4]. Simplified wind tunnel models were used to analyse flutter and design recommendations were made in this seminal work. In the 1930's, with the availability of better engines and in attempts to set new flying speed records, flutter began to be recognized as a critical safety hazard. Consequently, serious engineering effort in analysing and preventing flutter began in earnest, especially in the design of the faster fighter aircraft of the 1930's and 1940's. The solution of increasing the structural stiffness was not always possible due to weight considerations. Experiments and analytical models revealed that the flight velocity at which flutter occurs and its characteristic frequency are as much effected by the mass distribution as stiffness and hence mass balancing of the wings, tails and control-surfaces began to be an integral part of aircraft construction. In 1935 von Schlippe became the first person to carry out resonance testing in flight to identify the critical flutter speed [6]. His method was to oscillate the aircraft component with a mechanical device while in flight. As the aircraft approached the critical flutter speed the resonant amplitude increased drastically. Hence the critical flutter speed could be deduced while flying at sub-critical speeds by plotting the amplitude of forced oscillations against the flight speed. The increase in aircraft speeds due to better power-plant technology and reduced weight of stronger materials further increased the importance of flutter during World War II. In Germany alone a total of 146 flutter incidents took place resulting in 24 crashes in 1945 [4]. The crash of the Lockheed Electra in September 29, 1959 and another in March 1960 have been attributed to inducement of wing

flutter by propeller whirl. Recent examples include Taiwan's IDF fighter, which crashed due to flutter of the horizontal tail during a high dynamic pressure flight-test in 1992, leading to the cancellation of the project. Later in the same year, a prototype of the state-of-the-art American fighter, F-22, crashed in a flutter related accident. In September 1997, a U.S. Air Force F-117 "Stealth" fighter crashed due to aileron/flaperon flutter on a primary lifting surface [7]. Every year many small aircraft, usually home-builts, continue to become casualties of flutter.

As the maximum flight speed of aircraft increased beyond the speed of sound, it was noticed that flutter was most likely in the transonic range due to the unsteady motion of a shock wave on top of the wing. A better modelling of the unsteady aerodynamic loads in the transonic regime became possible with developments in computational fluid dynamics. At the same time, experimental facilities at organisations such as NASA-Langley Research Center were upgraded to study transonic flow phenomena [8]. The 16-Foot Transonic Tunnel has supported most major U.S. military programs both in their developmental stage and in on-going propulsion integration research.

One of the most famous cases of destructive flutter befell not an aircraft but a bridge, the Tacoma Narrows Bridge, then the third longest suspension bridge in the world in 1940. On November 7, only six weeks after the bridge opened, a steady 42-MPH wind was blowing when a cable near mid-span snapped, creating an unbalanced condition. The bridge collapsed after half an hour of twisting and bending [9]. Even today the exact mechanism of the flutter of the Tacoma Narrows Bridge is a subject of technical debates amongst engineers and scientists. The fact that half a century of analysis has not settled the question gives an idea of the complex nature of flutter.

1.2 Analysis Techniques

Aircraft flutter prediction has been carried out with the help of various techniques namely analytical means, tests on physical models and more recently by numerical simulations on computers. The decision as to which of these is to be used depends on a number of factors such as experience in a particular technique, the facilities available, the margin of safety for the flutter, structural configuration and the funds allocated for the project. Flutter occurs at a critical (or flutter) speed V_f which is defined as the lowest airspeed at which the aircraft structure will oscillate with a self-sustained simple harmonic motion. Flights at speeds above and below the flutter speed yield unstable and stable conditions respectively. The classical approach in flutter analysis is to assume that the motion is sinusoidal and of low amplitude, determine the aerodynamic forces for the condition and then solve for the roots of the characteristic polynomial arising from the assumed neutrally stable description of the equation of motion. Upon examination of these roots, a judgment is made as to whether the assumption of neutral stability was correct or not. Thus a root corresponding to a decaying or stable condition is considered to belong to a point below the flutter speed. A root corresponding to a divergent oscillation is assumed to belong to a point beyond the flutter speed and the root corresponding to neutral stability gives the flutter point. To obtain a solution of the flutter problem various values of reduced frequencies are assumed since this is the parameter for which the variation of the aerodynamic forces is known. By plotting the roots at these assumed frequencies, the point of neutral stability is obtained. This is one of the common forms of flutter analysis [10][11]. The U-g form of flutter analysis is the most common one in use in the USA. In this approach artificial structural damping is introduced by multiplying the squares of structural frequencies by $1+ig$ where g is the damping parameter. Pure sinusoidal motion is assumed. For a given flight velocity the g required to sustain sinusoidal motion for each mode is calculated. If

the value of g is equal to the real value then the velocity at which it occurs is the flutter point [11].

Flutter tests on physical models in wind tunnels are the most common means of obtaining data for validation and improvement of the aerodynamic modelling [12]. The behaviour of the small scale models in the wind tunnel testing can be related to the full scale aircraft by expressing the aeroelastic equations in non-dimensional form or by using dimensional analysis. An exact relation cannot be expected due to scaling effects. Flutter involves accelerated motions and hence mass effects in the fluid are of importance. For realistic simulation the ratio of fluid density to the model density has to be the same as that of the prototype. This introduces practical difficulties in the building of the model as the real aircraft is built with minimum weight and maximum stiffness which cannot be reproduced in the smaller scaled model. Even if the same materials are used as in the prototype the skin gauge, the size of the rivets and spar and rib dimensions will require some deviation in scaling causing differences in the ratio of fluid density to the model density. To make the wind tunnel results more representative in the transonic regime the concept of using full scale flexible components for testing is being explored and implemented. For low speed flutter tests the flutter boundary is usually approached by increasing the flow velocity in suitable increments. For high speed (compressible) flows the flutter boundary is approached by keeping the Mach number fixed and changing the stagnation pressure, and hence the dynamic pressure, in suitable increments [11].

In recent years with the advent of high speed digital computers and increase in computational resources the prospect of using numerical simulation for aircraft flutter analysis has become quite attractive. Yet most of the flutter computations in industrial applications use finite element based codes like MSC/NASTRAN^{TM} and NISA^{TM} which are based on linear aerodynamic modelling and hence are limited to subsonic and supersonic flow regimes. A non-linear Euler/RANS based numerical scheme is required for flutter analysis in transonic flows to take into account shock

TECHNIQUE	RELATIVE COST	BREAK DOWN
Analysis	29 %	29 %
Wind Tunnel	27 %	
Ground Vibration Test	19 %	71 %
Flight Flutter Test	25 %	

Table 1.1: F-14 Flutter Prevent Program [11]

induced non-linearities. Until now these coupled aerodynamic/structural dynamic computations have required considerable computational time and consequently, testing of rigid models in transonic wind tunnels has been used to generate corrections to aerodynamics predicted by linear methods. Because the design of a wind tunnel flutter model and the analysis of the corresponding data require substantial effort, it has been suggested that CFD based nonlinear aeroelastic simulations could be used if it is proved to be practical, fast enough and reliable [13]. Table 1.1 shows the breakdown of costs involved in a Flutter Prevention Program for the F-14 fighter aircraft [11]. A substantial percentage of overall costs went into physical testing. This component could be reduced by using computational techniques [13].

1.3 Linear Methods and their Limitations

Most of the commercial aeroelastic codes are based on a linear aerodynamic model. The reasons for this are speed, extensive experience in use, ease of implementation and awareness of validity and limitation of the computed results. Hence as compared to recent non-linear approaches the linear methods have been widely applied in industry. However, this approach has shortcomings which will be discussed in this section. There are two main assumptions in a linear aeroelastic scheme:

- The structure undergoes elastic harmonic motion with small amplitudes.

- The flow is approximated by a linearized theory.

Using an approximation of the classical approach, the flutter problem can be stated as

$$\mathbf{M}\delta\ddot{\mathbf{x}}_s + \mathbf{D}\delta\dot{\mathbf{x}}_s + \mathbf{K}\delta\mathbf{x}_s = \mathbf{L}(\delta\mathbf{x}_s, \delta\dot{\mathbf{x}}_s) \tag{1.1}$$

where $\mathbf{M}$, $\mathbf{D}$ and $\mathbf{K}$ are the structural mass, damping and stiffness matrices respectively, $\delta\mathbf{x}_s$ is the wing deflection and $\mathbf{L}$ the aerodynamic loads. The structural damping, which is typically small for aircraft wings, is assumed to be proportional to stiffness (based on empirical evidence) giving

$$\mathbf{M}\delta\ddot{\mathbf{x}}_s + \mathbf{K}(1 + ig)\delta\mathbf{x}_s = \mathbf{L}(\delta\mathbf{x}_s, \delta\dot{\mathbf{x}}_s) \tag{1.2}$$

and also the structural vibration is assumed to be harmonic

$$\delta\mathbf{x}_s = \delta\mathbf{x}_{sk}e^{st} \tag{1.3}$$

where the real part of s determines the stability i.e. positive is unstable and negative is stable. The aerodynamic loads L are calculated using a linear method (eg. a panel method) which is used to linearly relate forces to the deflections using an Aerodynamic Influence Coefficient (AIC) matrix [14]. A number of methods have been developed to solve the equation (1.2) like Vg, pk and the determinant P methods [15]. The use of linear methods is applicable only in subsonic and supersonic flows. The methods break down at transonic flow conditions because of the presence of mixed subsonic-supersonic flows and the motion of shock waves across the surface of the body. This is unfortunate since most passenger aircraft cruise at transonic speeds. LCO is another transonic phenomenon. Bluff body oscillations, buffeting and high angle of attack maneuvers are all examples of conditions beyond the scope of linear aeroelasticity. Some attempts have been made to extend the linear methods for transonic flow prediction. This is mainly carried out by approximately modelling the non-linear aerodynamics based on correction of linear AICs. The transonic equivalent strip (TES) method is one of the methods based on two

corrective steps, one is the mean flow (chordwise) correction step and a phase correction (spanwise) step to a given steady mean pressure input from measured or computed data [16]. A modification of Doublet Lattice influence coefficients using the results from a Transonic Small Disturbance (TSD) code was proposed by Pitt and Goodman [17] and applied by Roberto and Olympio [18] to the F5-E fighter aircraft. Considerable advances have been made in the fields of non-linear methods. Robust and efficient algorithms are now capable of solving for complete aircraft configurations with ever decreasing amounts of time [13] and hence settling for linear methods is no longer necessary.

1.4 CFD Based Analysis

Non-linear methods are frequently based on Euler/RANS aerodynamic modelling. Codes like AERO-F and AERO-S have been used successfully to simulate aircraft flutter on a complete aircraft in a practical amount of time [13]. The code used in the current studies (PMB3D) is a parallel, multiblock Euler/RANS based implicit code [19].

In fluid-structure interaction problems the fluid solution is usually computed on an Eulerian coordinate system, whereas the structural part is solved in a Lagrangian system. A loosely coupled code will solve the fluid and structural parts using two separate codes with an interfacing system between them for the transfer of loads and deformation. The advantage of a loosely coupled code is that it can re-use well established fluid and structure codes. In a loosely coupled aeroelastic solver following a modal approach the mode shapes and frequencies of the structure are obtained in advance either numerically or experimentally. These are than used to obtain the structural response. The number of structural equations is reduced by an order of magnitude compared with using a direct FEM [20]. Both static and dynamic responses can be accurately computed to predict complex phenomenon

like flutter using the modal approach [21]. The disadvantages are that errors can be introduced during the transformation of information and sequencing between the codes and the accuracy of results depend on the number of modes used. In the direct approach the aerodynamic forces calculated by the CFD code is mapped on to the structural nodes. The CSD code then calculates the structural response which is interpolated back on to the CFD grid. The CFD code then again calculates aerodynamic forces and this continues until a defined convergence criteria is met. The direct approach has the advantage of being more accurate than the modal one and also, if the CSD and CFD solver are modularly coupled by an external mapping algorithm, the ability to choose and couple different CFD and CSD codes [22]. The disadvantage of the direct approach is that it is computationally expensive as lot of time is wasted in input and output of the CSD/CFD responses. Simultaneously coupled codes are those in which the equations of the fluid and structural solvers are combined into one. The cost of increased complexity and unwieldiness in handling are the major drawbacks of these codes.

One of the first non-linear transonic flutter analyses was developed by Borland and Rizetta [23] in 1982. The fluid motion was modelled using the Transonic Small Disturbance (TSD) equation and the structural deformation was represented by the modes of the structure. Their procedure was incorporated in the loosely coupled aeroelastic code XTRAN3S. Cunningham et. al [24] further developed the TSD technique resulting in a new code called Computational Aeroelasticity Program-TSD (CAP-TSD). The equations for structural motion were based on the natural vibration modes of the structure. Schuster et al [25] used a Navier-Stokes aerodynamic model to formulate the aeroelastic problem on a complete fighter aircraft configuration using the solver ENS3D, but the analysis was limited to static aeroelasticity. Rausch and Batina [26] used a modified RANS code CFL3D to calculate wing flutter using Navier-Stokes aerodynamics on the AGARD 445.6 wing. Guruswamy and Byun [27] introduced the method of direct coupling of plate FEM model with

an Euler aerodynamic solver in 1993. A domain decomposition method where the structural and fluid solutions are calculated in separate modules was developed . Melville carried out an aeroelastic simulation of the F16 aircraft and the exercise correctly predicted two flutter onset points in good agreement with the test data [28]. In 2002 Farhat et al [13] applied the three field Arbitrary Lagrangian-Euler (ALE) formulation of the Euler and Navier-Stokes equations over an F-16 aircraft using a detailed structural FEM model.

1.5 Basis and Overview for Current Work

The current work is an extension of the work done by Goura [14]. At the start of the project an aeroelastic solver based on an Euler/RANS solver PMB3D, capable of both static and dynamic analysis, was developed. It

was tested and evaluated on the MDO and AGARD 445.6 wing cases and the results were shown to be comparable with the best computed results published[14]. A transformation scheme, the Constant Volume Tetrahedron technique, was proposed and implemented in the code. The main objective of the current work is to evaluate the transformation scheme on an aircraft geometry. On an aircraft there are number of structural components and each of these should correctly drive the corresponding fluid surface grid patches without introducing holes or kinks at the interfaces.

The project details are explained in the following four chapters of the thesis. Chapter 2 contains a description of the different transformation techniques available. Chapter 3 describes the CAD, structural and fluid models that were developed for the aeroelastic analysis. Chapter 4 explains the CVT methodologies implemented for the aircraft test case and Chapter 5 gives the conclusions of the current project and suggestions on future extensions.

Chapter 2

Transformation Methods

2.1 Introduction

In computational aeroelasticity the prediction of flutter boundaries requires calculating the flow around the flexible aircraft. Specialised computational codes for structural dynamics are finite element based and the fluid dynamic codes are finite volume based. To combine these two separate schemes into one single solver is usually considered impractical. Most of the modern computational aeroelastic codes solve for the structural response of the aircraft on a separate structural grid using a Computational Structural Dynamics (CSD) solver and the flow around the body on a fluid grid using Computational Fluid Dynamics (CFD). Since the grids for these two methods do not coincide at the structure-fluid boundary (interface) an interpolation scheme is required for the accurate transfer of structural information (displacements) from the structural to the fluid grid and the transfer of aerodynamic information (pressure, force) from the fluid grid to the structural grid at each time step. The global system defined by the union of the fluid and the structure subsystems being a closed system, it follows that at any time t, the reaction of the system is equal to the action of the fluid, and the energy released (except for the eventual structural damping) or absorbed by the structure is equal to the energy gained or

released by the fluid. Therefore it is desirable that the fluid and structure loads computed on the fluid surface grid and structural grid respectively also verify this property. Clearly, if the fluid and structure meshes have non-matching discrete interfaces, and/or the fluid and structural solvers employ different discretisation methods then the sum of the discrete loads on the structural elements interpolated from the fluid surface grid might not exactly match the loads computed on the fluid surface grid[29]. The structural deformation depends directly on the surface loads and in high fidelity Euler/Navier-Stokes calculations the solution is sensitive to the surface geometry. Hence it is of up most importance for accurate coupled flow calculations that minimum error is introduced during transformation between the grids. Due to the linear assumptions often made for aeroelastic calculations the panel methods and double lattice methods have been popular. These methods model the aircraft components as thick bodies and plates where primary deformation is bending and torsion with negligible in plane movement. Hence the transformation schemes developed have been influenced by this and have neglected the dilatation. These schemes are now briefly reviewed.

2.2 Interpolation Schemes

2.2.1 Infinite Plate Spline

The Infinite Plate Spline method developed by Desmarais and Harder [30] a widely used forms of spline methods used. Consider an infinite plate on which the structural points are located, having deflections δz_i. The static equilibrium equation for the plate is given by

$$\mathcal{D}\nabla^4 \delta z = q \tag{2.1}$$

where $\mathcal{D}$ is the plate flexibility and q is the distributed load. The solution for plate deflection can be written as

$$\delta z(x,y) = a_0 + a_1 x + a_2 y + \sum_{i=1}^{N} \mathcal{F}_i r_i^2 \ln r_i^2 \tag{2.2}$$

where r_i is the distance of any point (x, y) on the plate from the structural point $(x_{s,i}, y_{s,i})$. To produce linear behaviour at the infinity the force and momentum satisfy

$$\begin{aligned} \sum \mathcal{F}_i &= 0 \\ \sum x_i \mathcal{F}_i &= 0 \\ \sum y_i \mathcal{F}_i &= 0 \end{aligned} \tag{2.3}$$

From the Equations (2.3) the coefficients $\mathcal{F}_i$ are calculated for known displacements at the structural nodes. These are then back substituted into Equation (2.2) to determine δz for the unknown deflections at the aerodynamic grid points.
In the above explanation all the aerodynamic grid points were assumed to lie in the same plane as the structural grid. If the structural and aerodynamic points do not lie on the same surface then they are projected onto a neutral plane. The deflections for the projected aerodynamic points are calculated and then the original offset is added to the projected points to recover the deflected aerodynamic points.

2.2.2 Finite Plate Spline

This method was developed by Kari Appa [31] and applied by Guruswamy and Byun [27] to a fighter aircraft wing. The method makes use of a virtual surface (VS) which lies between the structural and fluid grids. The VS is discretisation into finite elements which are not necessarily the same elements as on the structural grid. A set of constraints are established such that the deformed VS is forced to pass through the deformed structural surface nodes. Consider m aerodynamic points at

which displacements are needed due to displacements at n structural points. For any element the displacement at any point in the element is given by

$$r = \Omega \mathbf{n} \tag{2.4}$$

where Ω is the shape function of the element at a point used to interpolate the displacements within an element in terms of the nodal degrees of freedom $\mathbf{n}$. The vector $\mathbf{n}$ can be related to the global displacement vector $\mathbf{q}$ by the connectivity matrix $\mathbf{A}$, hence the ith element can be stated as

$$\mathbf{n}_i = \mathbf{A}_i \mathbf{q}. \tag{2.5}$$

Using the above relation in Equation (2.4) the displacements vector for structural constraint points can be written after assembly, as

$$\mathbf{q}_s = \Psi_s \mathbf{q} \tag{2.6}$$

where

$$\Psi = \begin{bmatrix} \Omega_1 A_1 \\ \Omega_2 A_2 \\ \vdots \\ \Omega_n A_n \end{bmatrix}. \tag{2.7}$$

Similarly the displacement vector $\mathbf{q}_a$ at the aerodynamic points in terms of global displacement vector $\mathbf{q}$ can be written as

$$\mathbf{q}_\mathrm{a} = \Psi_a \mathbf{q} \tag{2.8}$$

where Ψ_a is the displacement mapping matrix from the VS to the fluid surface grid. To force the VS to pass through a given set of displacements $\mathbf{q}_s$ the penalty method of constraints (as described in [32]) gives the equilibrium state of the structure.

$$[\mathbf{K} + \delta \Psi_s^t \Psi_s]\mathbf{q} = \delta \Psi_s^t \mathbf{q}_s \tag{2.9}$$

where $\mathbf{K}$ is the stiffness matrix of the VS, Ψ_s is the displacement mapping matrix of the VS to the structural grid, and δ is a penalty parameter. Solving for $\mathbf{q}$ and

substituting in Equation 2.8, the displacements at the fluid surface grid points can be expressed as

$$\mathbf{q}_a = \mathbf{T}\mathbf{q}_s \tag{2.10}$$

where

$$\mathbf{T} = \Psi_a(\delta^{-1}\mathbf{K} + {\Psi_s}^T\Psi_s)^{-1}{\Psi_s}^T \tag{2.11}$$

2.2.3 Inverse Isoparametric Mapping

The isoparametric mapping technique is widely used in FEM analysis to transform state variables like displacement, stress and loads from structural grid points to the aerodynamic grid points. In this approach the same shape function (N) is used to interpolate the aerodynamic grid point and to approximate the structural deformation. The isoparametric mapping is from a local coordinate (ξ, η) to a global coordinate system (x, y). The mapping of an aerodynamic point is defined by the shape functions for a structural element within which it lies. Consider an aerodynamic point lying in a quadrilateral structural element (Figure. 2.2.3). The local coordinates for such a point can be defined as

$$x = \sum \mathbf{N}_i(\xi, \eta)x_i \; 1 \leq i \leq 4 \tag{2.12}$$

$$y = \sum \mathbf{N}_i(\xi, \eta)y_i \; 1 \leq i \leq 4 \tag{2.13}$$

where

$$\begin{aligned}
\mathbf{N}_1(\xi, \eta) &= 1/4(1 - \xi)(1 - \eta) \\
\mathbf{N}_2(\xi, \eta) &= 1/4(1 + \xi)(1 - \eta) \\
\mathbf{N}_3(\xi, \eta) &= 1/4(1 + \xi)(1 + \eta) \\
\mathbf{N}_4(\xi, \eta) &= 1/4(1 - \xi)(1 + \eta)
\end{aligned} \tag{2.14}$$

After calculating the global transformed aerodynamic coordinates the local coordinates (ξ_m, η_m) of the aerodynamic points on the deformed structural grid are

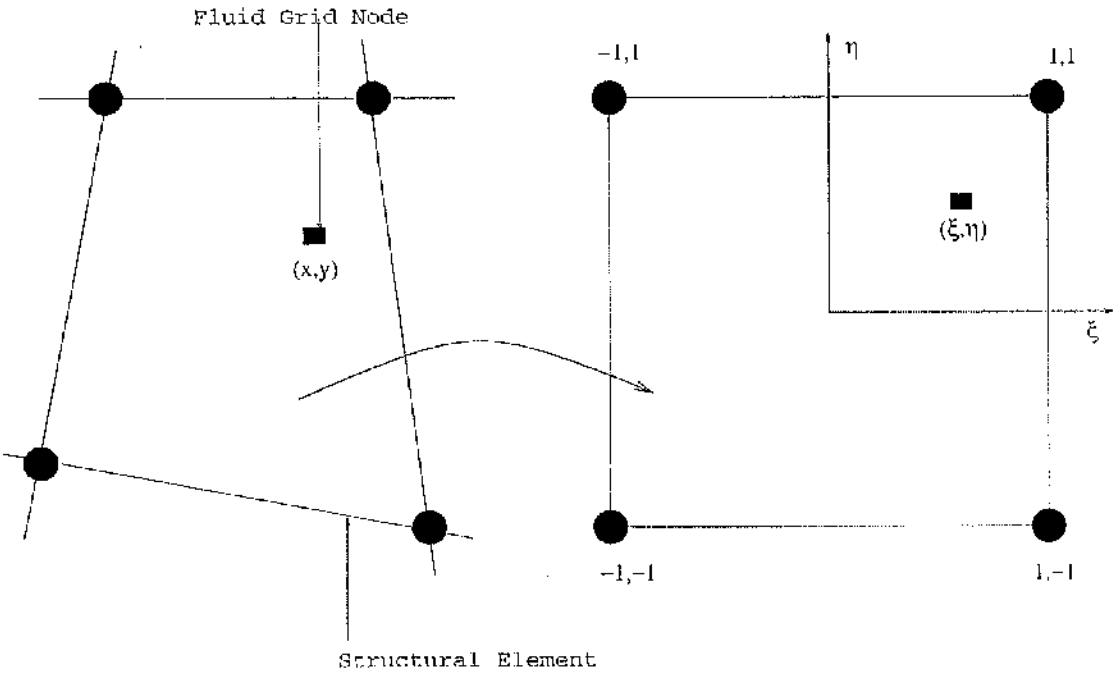

Figure 2.1: Isoparametric Transformation

calculated as follows. An arbitrary line PQ is defined such that it lies on the aerodynamic point M and on an element node P. The line transforms into P'Q' through inverse mapping. The equation for the line P'Q' can be written as

$$A\xi^2 + B\xi + C = 0 \tag{2.15}$$

where the coefficients are constants calculated from the shape functions and the coordinates-ordinates of the elemental nodes [33]. Once the local coordinates-ordinates for the transformed aerodynamic grid point (ξ_m, η_m) are calculated then the transformed planar displacements (u, v) are obtained by isoparametric mapping

$$u = \sum_{i=1}^{n} \mathrm{N}_i(\xi, \eta) u_i \; 1 \leq i \leq 4 \tag{2.16}$$

$$v = \sum_{i=1}^{n} \mathrm{N}_i(\xi, \eta) v_i \; 1 \leq i \leq 4. \tag{2.17}$$

The aerodynamic loads can be distributed by using the (ξ, η) values. This form of

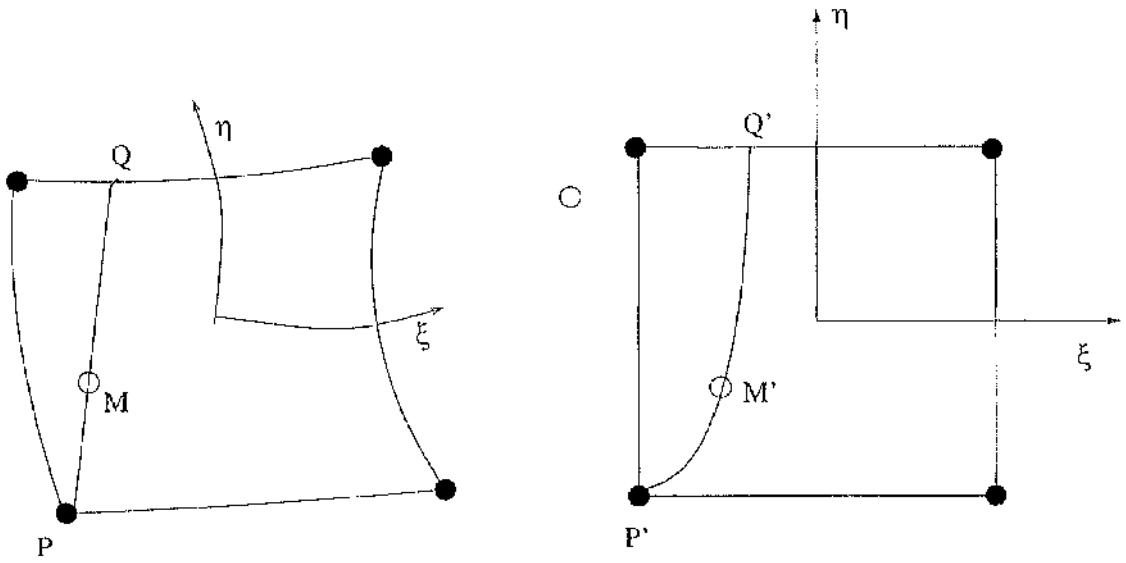

Figure 2.2: Transformation of line PQ

transformation is accurate but suffers from a drawback that the aerodynamic points and the structural points must lie on the same surface.

2.3 Boundary Element Method

The transformation methods described earlier work on the fluid surface grid and structural grid. Chen and Jadic [34] proposed a BEM solver based on the full three dimensional equilibrium equations that would effectively transfer loads and displacement between the structural and fluid grids. In this approach the fluid surface grid is considered as an elastic homogeneous body with the fluid points as the nodes of the external boundary and the structural grid nodes are the internal points of the body as shown in Figure 2.3. A minimum strain energy requirement results in the universal spline matrix S that relates the force and displacement

vectors between the CFD and CSD grids as

$$\mathbf{u}_a = \mathbf{S}\mathbf{u}_s \tag{2.18}$$

$$\mathbf{f}_s = \mathbf{S}^T\mathbf{f}_a \tag{2.19}$$

where $\mathbf{u}_a$ and $\mathbf{f}_a$ are the fluid grid node displacements and loads and $\mathbf{u}_s$ and $\mathbf{f}_s$ are the displacement and loads on the structural grid nodes. The universal spline matrix $\mathbf{S}$ is obtained as follows. The usual BEM approach is to obtain an integral form of the equilibrium equation relating the internal displacement with the displacement and loads at the boundary Γ. The equilibrium equation in terms of displacements in tensor notations is written [35] in the form

$$[1/(1-2\nu)]u_{j,jl} + u_{l,jj} = 0 \tag{2.20}$$

where ν is the Poisson's ratio. The result of Equation 2.20 is known as the Somigliana's identity [35] and is written as

$$u_k^i + \int_\Gamma p_{ik}^* u_k d\Gamma = \int_\Gamma u_{ik}^* p_k d\Gamma \tag{2.21}$$

The superscript i refers to an internal point and superscript * refers to a Kelvin solution. The boundary of the body Γ is discretised into boundary elements and now Equation 2.21 can be written in the matrix form as

$$\mathbf{u}_s + \mathbf{H}_{bi}\mathbf{u}_a = \mathbf{G}_{bi}\mathbf{p} \tag{2.22}$$

where $\mathbf{p}$ are the surface loads and the subscript bi refers to the boundary-interior influences. For the points on the boundary the relation between the displacement and the loads is given by

$$\mathbf{H}_{bb}\mathbf{u}_a = \mathbf{G}_{bb}\mathbf{p} \tag{2.23}$$

Here bb refers to the boundary-boundary influence. Substituting for $\mathbf{p}$ from Equation (2.23) in Equation (2.22) we have

$$\mathbf{u}_s = \mathbf{B}\mathbf{u}_a \tag{2.24}$$

where

$$\mathbf{B} = \mathbf{G}_{bi}\mathbf{G}_{bb}^{-1}\mathbf{H}_{bb} - \mathbf{H}_{bb} \tag{2.25}$$

Equation (2.24) can be used only if the number of internal points (the structural grid) is equal to the boundary points (fluid grid), but in practice the structural grid is almost always coarser than the fluid grid. To obtain the universal spline matrix a minimisation of strain energy approach was used. The strain energy function ϵ can be obtained as

$$\epsilon = \mathbf{u}_a^T \mathbf{R}_a \mathbf{p} \tag{2.26}$$

where $\mathbf{R}_a$ is the matrix containing the areas of the boundary elements. Substituting for $\mathbf{p}$ in Equation (2.26) we have

$$\epsilon = \mathbf{u}_a^T \mathbf{A} \mathbf{u}_a \tag{2.27}$$

where

$$\mathbf{A} = \mathbf{R}_a \mathbf{G}_{bb}^{-1} \mathbf{H}_{bb} \tag{2.28}$$

A Lagrange multiplier technique is applied to minimise the strain energy. An objective function is defined as

$$\mathbf{F} = \mathbf{u}_a^T \mathbf{A} \mathbf{u}_a - \lambda^T (\mathbf{u}_s - \mathbf{u}_{s,given}) \tag{2.29}$$

where λ is the Lagrange multiplier and $\mathbf{u}_{s,given}$ are the given values of the displacements. By minimising the function in Equation (2.29) such that

$$\frac{\partial \mathbf{F}}{\partial \mathbf{u}_a} = 0 \tag{2.30}$$

with the constraints

$$\mathbf{u}_s = \mathbf{u}_{s,given} \tag{2.31}$$

we get an expression for the universal spline matrix $\mathbf{S}$ as

$$\mathbf{u}_a = \mathbf{S}\mathbf{u}_s \tag{2.32}$$

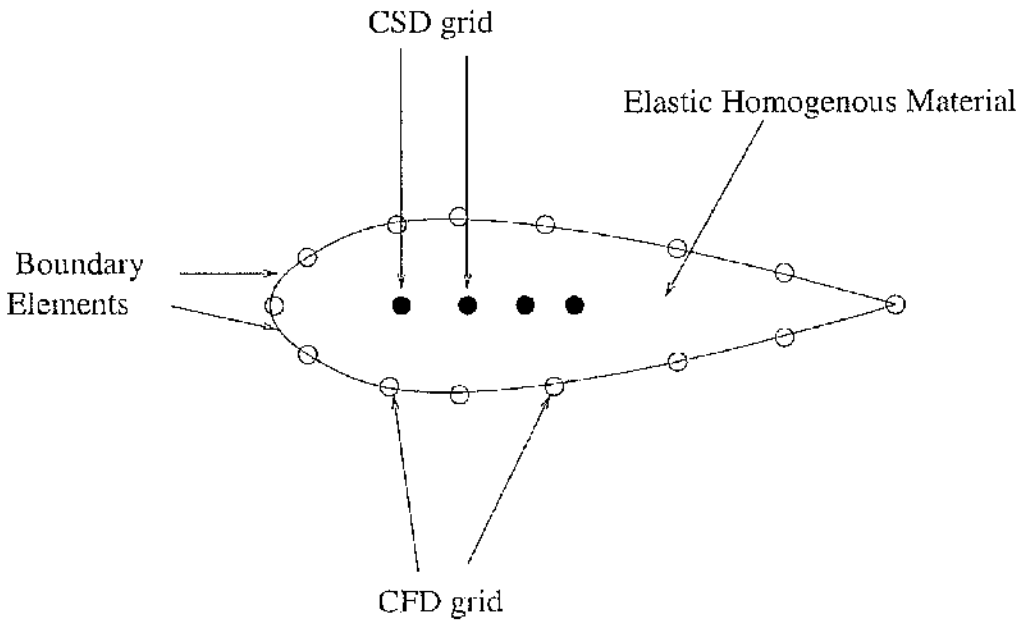

Figure 2.3: BEM treatment of an aerofoil

2.4 Melville's Method for Complete Aircraft

A method dedicated to complex geometries was proposed in [28]. The principle is that when the structural model is composed of simplified components like beams and plates then it is important to drive the motion of an aerodynamic grid point from the correct structural component. Each component is given associated shape functions which are used to transfer the structural displacements to the relevant aerodynamic points via a least squares fit. A hierarchy of components is defined which reflects the way these are connected. For example, the fuselage motion is considered independent of the rest of the aircraft and so is transformed first. Next, the wings are attached to the fuselage and so the wing displacements are assumed to be the sum of a rigid motion due to the fuselage and an increment due to the elasticity of the wing. The rigid motion is first applied, ensuring a contiguous surface is preserved at the wing root, and then the increment is interpolated via the mode shapes. A typical error of 10 % is quoted [28].

2.5 Evaluation for Complete Aircraft Configurations

Realistic aircraft configurations need to be analysed for computational aeroelasticity to realise its potential. This involves solving the transformation problem. There are two aspects to this. First, there is a need to treat aerodynamic and structural surfaces which are offset due to simplifications in the structural model. Secondly, multi-components need to be transformed without introducing holes in the aerodynamic surface.

2.5.1 Structural Simplifications

To illustrate the difficulty of simplified geometries, consider modelling a wing by a plate for structural purposes. For the IPS method the aerodynamic points are projected onto the plate. The spline matrix is then used to transform the projected points and finally the aerodynamic points are recovered by adding the original out-of-plane displacement to the new positions for the projected points. The problem with this approach is with the out-plane treatment, as illustrated in Figure 2.4 from [14]. A distortion is introduced which increases with the size of the displacements.

It was this problem which motivated the development of the BEM based method in [34]. This method copes very naturally with mismatching surfaces. The isoparametric method is not applicable when the surfaces do not coincide.

A second issue identified as important and arising from structural simplifications is when the plate planform does not match that of the wing. This arises when the load bearing wing box is used to define the structural plate. It was shown in [14] that extrapolation beyond the definition of the plate should be linear and using the IPS introduces a spurious camber into the wing which can seriously change the dynamic and static response. The mode shapes used in [28] were constructed with this consideration in mind.

2.5.2 Complex Geometries

The work presented in Farhat [13] used a detailed FEM model for the F16 which conforms fully to the true geometry used for the aerodynamic grid. This means that the isoparametric mapping is a natural and successful method for the transformation and the complex geometry does not introduce any additional mapping complication. The BEM method in principal can also deal with a complex geometry without complication.

Melville constructed his method to deal specifically with a complete aircraft configuration. He noted some errors in the reconstructed geometry, probably arising from the reconstruction via mode shapes. However, the strength and insight of the method is the definition of a hierachy of components and the use of this to match transformed components, avoiding holes.

We have been unable to find an example of the Infinite Plate Spline method used for complex geometries.

2.5.3 Practicality of Method

An important consideration is that complete aircraft models involve large CFD and CSD grids. The practicality of the method is therefore crucial. For the example presented in the next chapter there are thirteen thousand fluid points on the aircraft ($n_a = 13000$) and 1700 structural points ($n_s = 1700$).

For the IPS and FPS methods a matrix defining the transformation must be stored. The number of elements in this matrix is $9 \times n_a \times n_s$, which means around 200 million non-zeros for the example in the next chapter. The BEM method requires even more memory. The isoparametric and Melville methods do not suffer from this overhead.

2.6 Evaluation

When the structural and aerodynamic surface grids are defined on the same surface then the use of an isoparametric mapping is entirely satisfactory, as shown in the work of Farhat [13]. However, when the structural model is built from simplified components, as is the normal practice in industry, then a completely satisfactory transformation for large displacements is not available. First, IPS, FPS and BEM based methods require large amounts of memory. It is also not clear how to apply the IPS method over the different components without introducing a mismatch between components. The method of Melville copes well with the complex geometry but the accuracy for each component individually was called into question.

There is therefore a need for a cheap and precise transformation method for aircraft geometries. This will be considered in Chapter 4.

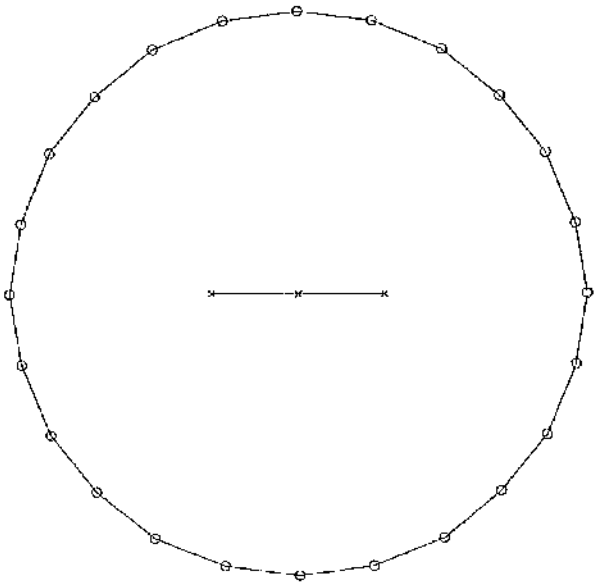

(a) Initial

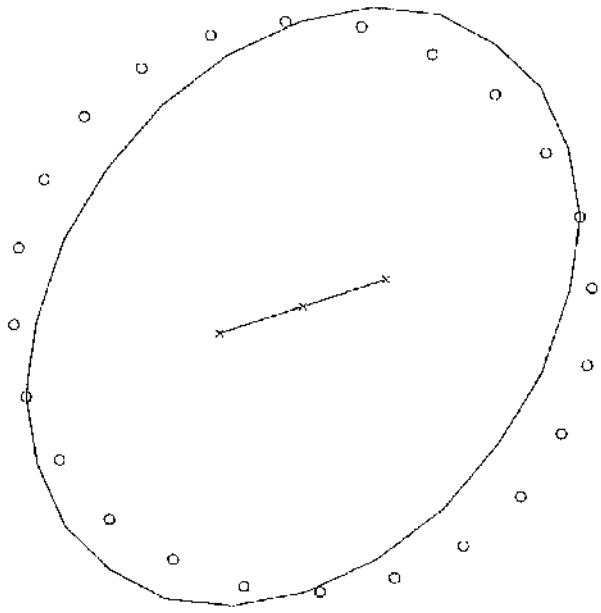

(b) 0.1π

Figure 2.4: Rigidly rotated circle. Solid lines are the recovered fluid points by IPS [14]

Chapter 3

The Aircraft Test Case

Transformation is tested on the Structural Dynamics Model (SDM) obtained from the Institute of Aerospace Studies-Canada [36]. The SDM model was originally constructed for experimental studies on fin buffet, and the dimensions are similar to a scaled down version of the F16 aircraft. The computational model constructed was scaled up again to realistic aircraft dimensions. The SDM CAD model was supplied in the form of 2D AUTOCAD drawings. A number of stages was involved before a final CAD model was obtained from these 2D drawings. This included the construction of a 3D wireframe model, a 3D solid model of each component and finally assembly of all the solid model components into a complete aircraft. Construction of a wireframe model was necessary because of the need to validate the dimensions of the solid model. A brief description of the SDM model is given in the next section. The structural model is a combination of 2D and 1D components and lives inside the fluid surface grid and is typical of the structural modelling approach often taken in practice. The plates and beam are given material properties such that the modes mimic the behaviour of a detailed model. Finally, the construction and testing of the fluid volume grid is described.

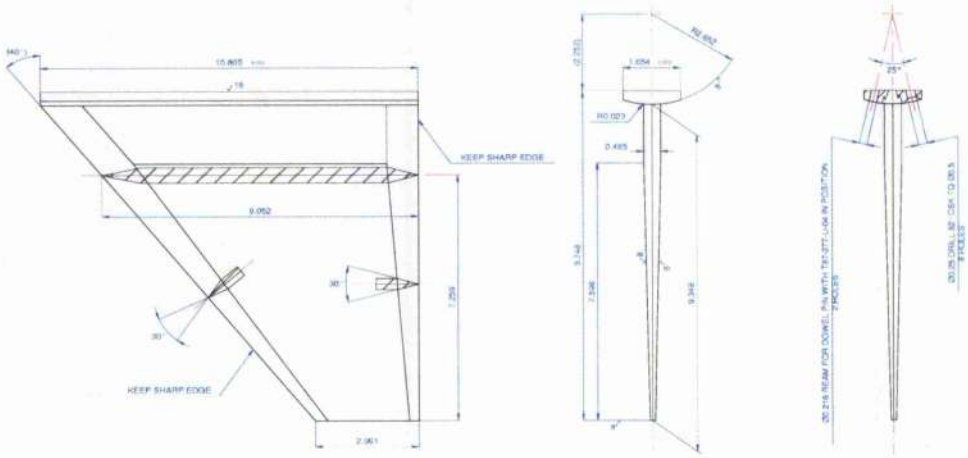

Figure 3.1: 2D drawing of the wing [36]

3.1 The CAD Model

3.1.1 The SDM Model

The 2D drawings were provided in the AUTOCAD .dwg format. The drawings are of the components of the aircraft as seen from different views i.e. plan view, top view and side view. The dimensions are in feet and inches. Some of the major components of the aircraft are described below.

Figure 3.1 shows the 2D AUTOCAD drawing of the wing with dimensions still in feet and inches. This drawing shows only the main body of the wing with the leading edge extension, just below the cockpit, missing. The missing component was constructed on the whole model by manually measuring the dimensions from the 2D drawing of the complete aircraft (see Figure 3.2). The wing has sharp leading and trailing edges and the absolute thickness of the wing decreases from the root to the tip.

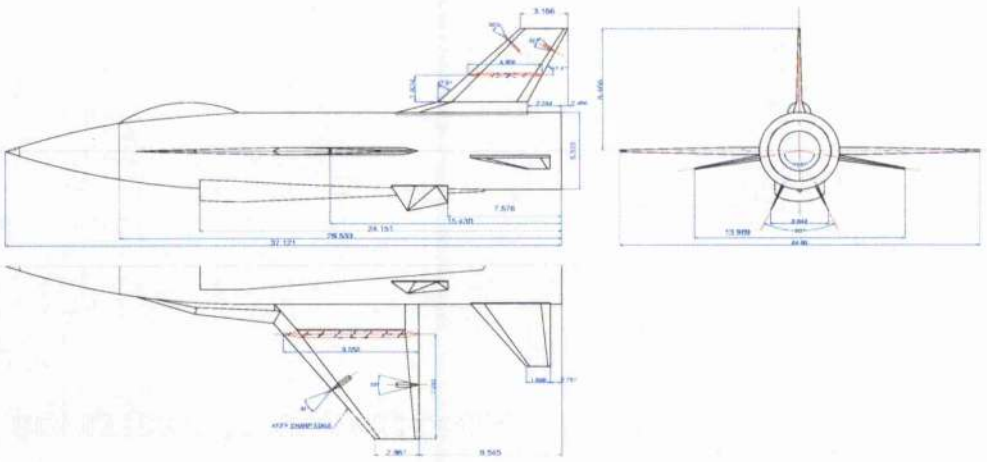

Figure 3.2: The top, side and front views of the complete aircraft

The fuselage is a circular cylinder of diameter 1.62 m at the tail end. Since the original drawings are meant for construction of a physical model information regarding details such as the position for holes for nuts and depth of the grooves for attachments is included. These have been ignored in the 3D CAD model. The horizontal stabilizer is similar to the main wing in construction including the sharp leading and trailing edges. It is attached to the fuselage at an anhedral angle of 10° (see Figure 3.2).

3.1.2 Construction of the 3D Model

Using the 2D drawings a wireframe model of each component was constructed. Solid models of the components were constructed using the extrusion and rotation commands on basic shapes. Rough components were obtained which were then sliced using the coordinates from the wireframe models. Finally each solid component was fused with the others to give a complete 3D model of the aircraft. The operations carried out for the construction of each component are described below.

Nose

The tip of the nose of the aircraft was constructed by revolving a triangle of the given dimensions in AUTOCAD. The sleeve which forms the rear part of the nose was modelled by first creating a 2D polyline over the given shape and then revolving it. The complete nose was formed by fusing the tip and the sleeve into a single unit.

Fuselage

The 2D drawing of the fuselage contained a number of grooves and holes for the fixtures in the physical model. These were first modified and a clean outline was drawn because we do not require these for the current work. Next the lower half of the 2D drawing was erased up to the centre-line since the fuselage is symmetrical about its axis. Next a polyline was drawn over this and, using this as the axis, revolved 180° exploiting the symmetry.

Wing

The wing was constructed by first drawing a square box with thickness equal to the thickness and width of the wing at the root. The box was extruded to the span of the wing with a taper angle so that the thickness at the tip was the same as the thickness of the tip of the wing. The leading and trailing edges were then given shape by using the slice command in AUTOCAD. To take into account the curvature of the fuselage the wing root was extended by around 0.125 m so that when fusing with the fuselage there are no gaps formed. The wing geometry has a leading edge extension close to the fuselage and ahead of the wing for which details were not available separately. The only details available for this component were those on the 2D drawing of the complete aircraft (see Figure 3.2). This component was first modelled as a solid box and fused with the wing and fuselage. Then, using the coordinates from the 2D drawing, it was given shape using the slice command.

Tail Wing

The tail wing was constructed in a similar way to the wing but was attached to the fuselage at an angle of 10°. Like the wing the tail wing is extended 13 cm at the root before being fused with the fuselage to prevent the formation of any gaps.

Tail Fin

The tail fin was constructed in two parts. The upper part was similar in construction to the wings but the lower half has a block shaped structure. The upper part was constructed like the wing while the lower portion was first modelled as a block which was then sliced by using the coordinates from the 2D drawing.

Canopy

The canopy was not constructed using the actual dimensions due to the difficulty of the profile. Instead a bubble shape was constructed and fused with the fuselage. It is assumed that this approximation is valid since the canopy is expected to have only a small influence on the flutter calculations.

Assembly

Once the individual components were constructed they were fused to form the complete model. Taking the tip of the nose as the starting point the rest of the components were connected one by one in the following order. The fuselage was fused with the sleeve of the nose. Then the wings were placed at a location measured from the 2D drawing of the whole aircraft. The wings were placed so that the extra 0.13 m mentioned earlier were all inside the fuselage. Next, taking the side view, and keeping the nose as the centre, the whole of the aircraft was rotated by 10° and the tail wing was attached. The fuselage was rotated back to its original position and the vertical fin attached using the coordinates from the 2D drawing. Then the

canopy was fused with the fuselage. The complete 3D model was checked for its dimensions with the 2D drawings, and is shown in Figure (3.3)

Simplifications Made

As the original 2D drawings were meant for the construction of a physical test model and not a computational one the tolerance level used in the CAD files was high and hence some approximations were included in the measurements while using the higher tolerance level. Also geometrical approximations were made by ignoring the engine inlet, the two vertical fin like projections below the back end of the fuselage and the exact shape of the canopy. When carrying out these approximations we have tried to make a demonstration case which is representative of a fighter aircraft to test the transformation methods but which avoids complications during CFD mesh generation.

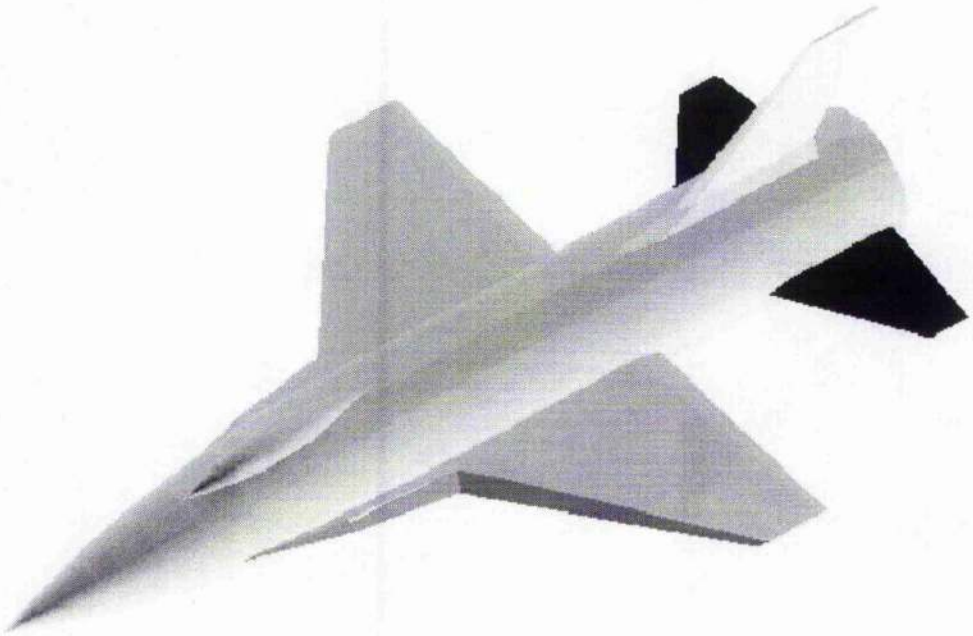

Figure 3.3: The complete 3D model of the aircraft

3.2 The Structural Model

Computational aeroelastic analysis involves two grids i.e. the fluid grid and the structural grid. The fluid grid is constructed over the actual profile of the model whereas the structural grid can be a simplified version of the actual geometry. The structural grid is simplified because a good structural representation can be obtained using plates and beams which are much easier to assemble. The current study is aimed at testing of the transformation scheme on a basic aircraft configuration devoid of external stores, control surfaces etc. It is conceivable that computational simulation of a more complete aircraft configuration could be performed, though it remains out of the domain of the current work. To test the transformation techniques three structural models were constructed with minor differences in each. Structural Model 1 has the fuselage modelled as a plate with the fuselage having freedom to twist. Structural Model 2 again has the fuselage modelled as a plate but this is constrained in torsion. Structural Model 3 has the fuselage modelled as a 1-Dimensional beam with twisting motion for the fuselage allowed.

The following sections explain the construction of the structural models and the modal frequency analysis carried out on them. The FEM pre and post processing software MSC-PATRAN was used for the construction and frequency visualisation whereas the FEM solver ABAQUS was used for frequency analysis. The model has been constructed to have a modal content similar to a full aircraft rather than the original rigid wind tunnel model (refer [36]) on which the current model is based.

3.2.1 Fuselage

As the structural model is the simplified version of the actual geometry a couple of simplifications were carried out on the different components of the aircraft. The fuselage for Models 1 and 2 is in the form of a plate with the front part ending in a point so that the structure lives inside the true aircraft profile. The fuselage

for Model 3 is modelled as a 1D beam. The different components are attached on the fuselage by stiff connectors. The connectors for the Model 2 have a boundary condition which limits their rotation with respect to the fuselage. The model static point of attachment is at the rear of the fuselage. Tables (3.1-3.3) give the material properties of the fuselage for the 3 models. The short connectors are made up of a single FEM element with two nodes. This is to ensure that during the transformation one of the nodes is included in the fuselage transformation scheme and the other in the scheme for the wings as discussed later.

3.2.2 Wings and Tail Plane

The wings, the horizontal stabilizer and the vertical fin are modelled as 2D thin shells. They are attached to the fuselage by 1D stiff connectors. The connectors could have been modelled as rigid elements instead, but little movement at the interface provides a good test for the weighting scheme used during the transformation (see Chapter 4). The size and dimensions of these structures are such that they are completely embedded in the full geometry of the aircraft. Tables (3.1- 3.3) give the material properties for the different components. The dimensions and material properties of the structural components are selected so that the modal frequencies and shape match those of the computed values for a similar test case given in [28].

3.2.3 Modal Frequencies

An FEM grid was constructed for the structural model using PATRAN. The 1D beams were discretized into two node elements and the 2D surfaces into triangular elements.

Member	Dimension	Thickness / Radii (m)	Density (kg/m^3)	Modulus of Elasticity (Pa)
Wing	2D Plate	0.1	700	5×10^{10}
Vertical Fin	2D Plate	0.1	700	5×10^{10}
Tail Plane	2D Plate	0.1	700	5×10^{10}
Fuselage	2D Plate	0.3	200	3×10^{10}
Connectors	1D Beam	0.1	400	1×10^{19}

Table 3.1: Material and Dimensional Properties of the Components for Model 1

Member	Dimension	Thickness / Radii (m)	Density (kg/m^3)	Modulus of Elasticity (Pa)
Wing	2D Plate	0.1	700	5×10^{10}
Vertical Fin	2D Plate	0.1	700	5×10^{10}
Tail Plane	2D Plate	0.1	700	5×10^{10}
Fuselage	2D Plate	0.5	250	3×10^{10}
Connectors	1D Beam	0.1	400	1×10^{19}

Table 3.2: Material and Dimensional Properties of the Components for Model 2

Member	Dimension	Thickness / Radii (m)	Density (kg/m^3)	Modulus of Elasticity (Pa)
Wing	2D Plate	0.1	700	5×10^{10}
Vertical Fin	2D Plate	0.1	700	5×10^{10}
Tail Plane	2D Plate	0.1	700	5×10^{10}
Fuselage	1D Beam	0.3	250	2×10^{11}
Connectors	1D Beam	0.2	200	1×10^{18}

Table 3.3: Material and Dimensional Properties of the Components for Model 3

It is important that the 2D surfaces have triangular elements as the CVT scheme uses a triangle on the structural grid and a node on the fluid surface grid to form

a tetrahedron for transformation (see Chapter 4). The different components are connected into a single entity by ensuring that the grid nodes at the connecting areas coincide for each component and then eliminating the duplicate nodes. Once the FEM grid was ready it was preprocessed in PATRAN and analyzed in the FEM solver ABAQUS for the modal frequencies.

It is usually the case that the vibrational modes greater than the first 10 natural modes are not important for the prediction of the onset of flutter. Usually the third anti-symmetric mode is the most significant mode. The first 4 modes of vibration were retained here to demonstrate the transformation scheme. These modes include the first and second fuselage bending modes and the first symmetric and anti-symmetric bending modes for the wings. The aircraft free-free modes that would include aircraft roll and pitch-plunge motion are not included as they are rigid body modes which are not needed to test the transformation. As experimental results for flutter on the F16 aircraft are not available in the literature the frequencies and mode shapes for the structural models in this study are evaluated against a similar study carried out by Melville [28]. Table 3.4 shows the frequencies for Melville's F16 model and frequencies of Structural Models 1, 2 and 3. Though the frequencies don't match exactly they are of the same order of magnitude and exhibit similar mode shapes. It should be stressed that the current work is not based on prediction of onset of flutter or simulation of flutter but on developing an effective technique for the transformation between the structural and fluid grids should such a simulation be carried out in future. The material properties used here for the structural response are arbitrary and fulfills the need of providing realistic mode shapes though of not exact frequencies. The Figures 3.5 to 3.7 show the different modes of the structural model.

	Melville's Study [28]	Structural Model 1	Structural Model 2	Structural Model 3
Symmetric Wing bending	6.2	10.148	11.588	9.0389
Antisymmetric wing bending	9.2	7.8348	10.092	9.8108
Fuselage lateral bending	-	5.173	9.3169	10.303
Fuselage vertical bending	-	14.064	9.3406	11.744

Table 3.4: Comparison of frequencies (Hz)of different models

3.3 The CFD Model

A bullet shaped computational grid was constructed around the aircraft model with farfield boundaries 2 aircraft lengths in the circumferential direction and 10 aircraft lengths from the inflow to the outflow boundary in the axial direction (see Figure (3.8)). As an Euler based solver is used for aeroelastic calculations in PMB3D a relatively shorter farfield boundary is thought to be sufficient.

The grid generation software ICEM-HEXA was used to generate a multiblock structured grid for the flow simulation. An O-grid blocking strategy is applied around the aircraft with the fuselage as the core and the blockings over the wings and tail plane formed by collapsing radial lines around the component. Figure (3.9) shows the front view of the aircraft blocking. The block lines seen in this figure have been taken from just ahead of the wing. An attempt has been made to smooth the blocks in the axial direction by tilting the block lines with respect to the fuselage at the angle of the wings. The slanting of block lines in such a manner has prevented any large angular differences arising between the adjacent blocks of the grid. The

cell spacings on the surfaces of the component are kept at 10^{-3} of the root chord length of the wing. Figure (3.4) shows section of the fine grid taken approximately at midway of the aircraft in the x-y plane. The fine grid consists of 5.14 million grid points and 536 blocks. A coarse grid is obtained from this fine grid by omitting every alternate grid point in the three directions. The grid thus obtained has 0.6 million grid points. Half model versions of the grids were used for the calculations which are discussed in the next section.

3.4 Flow Simulation

Inviscid flow simulation is first carried out using PMB3D on both the coarse and fine grids to make sure that there are no marked differences in the solutions. The symmetric case was run for Mach numbers 0.5 and 0.9 and at an angle of attack of 5°. Each case was run for 300 explicit steps and implicit steps with CFL numbers of 0.4 and 20 respectively. The results for Mach 0.5 on coarse and fine grids are shown in Figures (3.10) and (3.11) respectively and the results for Mach 0.9 on coarse and fine grids are shown in Figures (3.12) and (3.13) respectively. The residual converges about 5 orders for all cases. There is no marked difference between the results of the coarse grid and the fine grid for each of the cases. As expected for a 5° angle of attack test case, a high pressure region is obtained over the lower surface of the wings and the nose region for all the four cases. There is a marked difference in the pressure and density distribution between the Mach 0.5 and Mach 0.9 test cases. The pressure difference between the lower and the upper wing surfaces is larger for the Mach 0.9 case than the 0.5 cases. This leads to larger lift generated at the higher flow velocity. The region of low pressure above the canopy is due to the acceleration of the flow over the contour and is visible in both the cases. There are no wing tip vortices. There is a sharp density gradient visible at the trailing edge in the 0.9 Mach number test case. This could be a trailing edge shock or lack of grid density

to resolve the flow in that region. Though just before this shock there is a patch of low density region on both upper and lower surface of the wing which is caused by the flow accelerating along the bevelled trailing edge. The region around the cone at rear end of the aircraft shows density distortions and surface pressure on the cone itself is higher then the free stream pressure. The part of the cone below the x-axis shows higher pressure than the part above and there is a comparatively less dense region just before the cone starts. Again an explanation for this would be that for a given angle of attack the flow accelerates at the cone-fuselage interface and then slows down due to the cone geometry. In the final simulation a jet condition would be applied at the rear end of the aircraft so no cone would be necessary.

Summary

Validation data in terms of experimental results or from other similar computational studies are not available. Visual inspection of the results does not show any unexpected flow phenomena and hence taken to be valid. There are no marked differences in the solution for the fine and coarse grids for flows at Mach numbers 0.5 and 0.9. This suggests that a coarse grid could be used for the transformation studies. This brief evaluation indicates that the CFD volume grids and the structural models are of a reasonable quality in for the purpose of the current work, which is testing the transformation between grids.

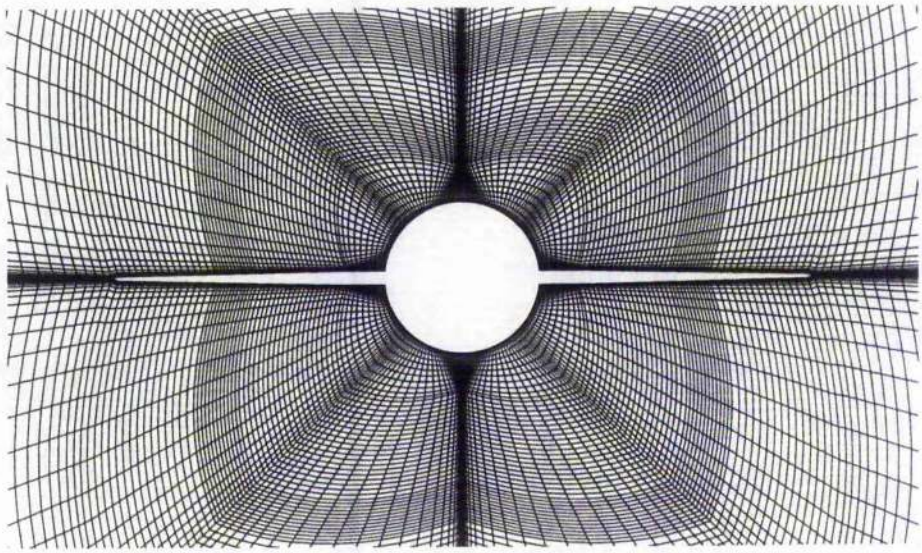

Figure 3.4: Sectional grid through x-y plane

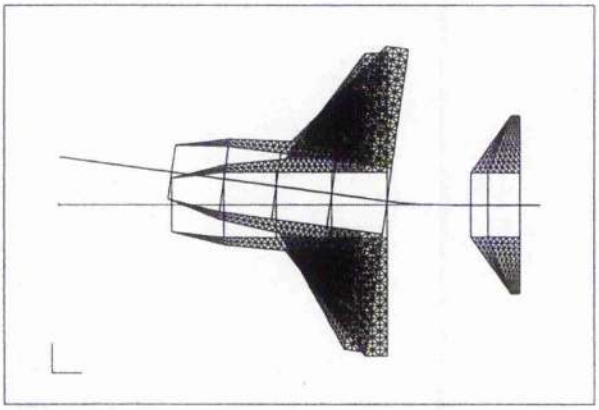

(a) Fuselage Lateral Bending

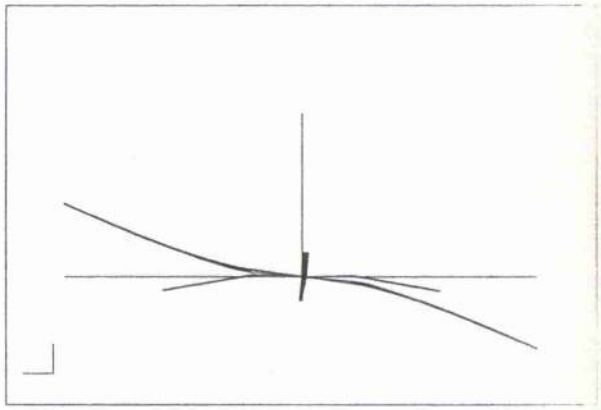

(b) Wing Antisymmetric

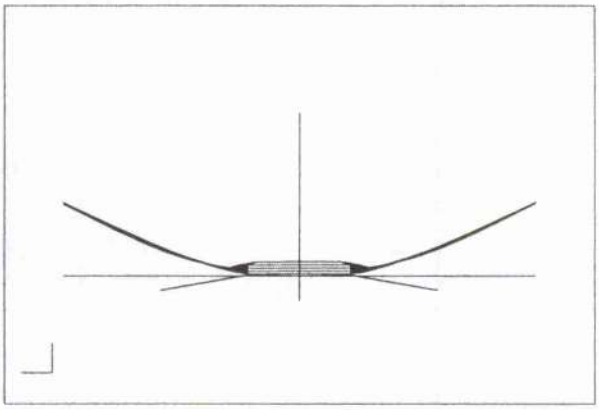

(c) Wing Symmetric

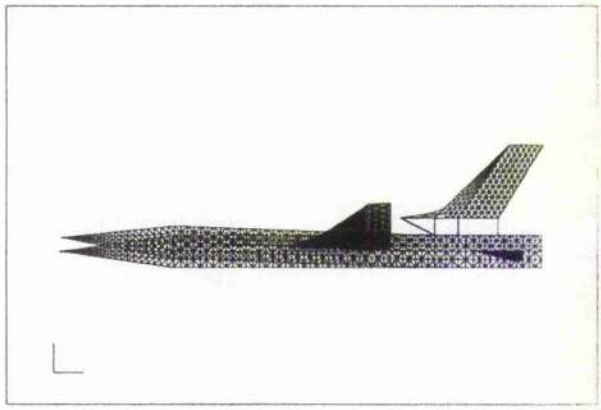

(d) Fuselage Vertical Bending

Figure 3.5: Modes for Structural Model 1

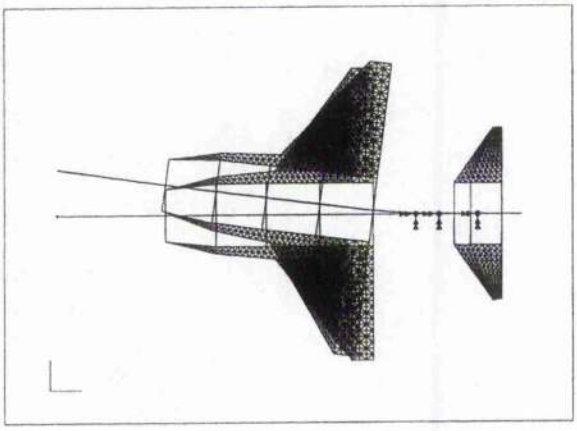

(a) Fuselage Lateral Bending

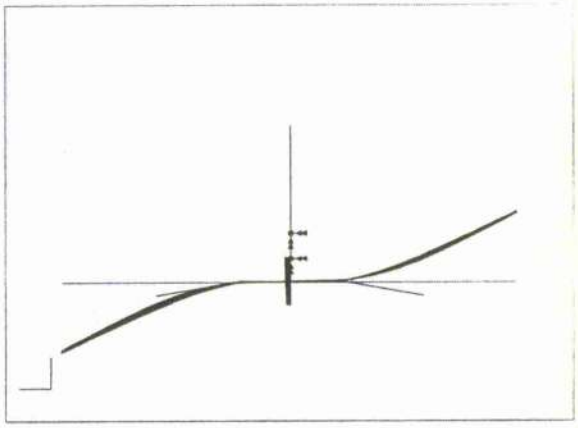

(b) Wing Antisymmetric

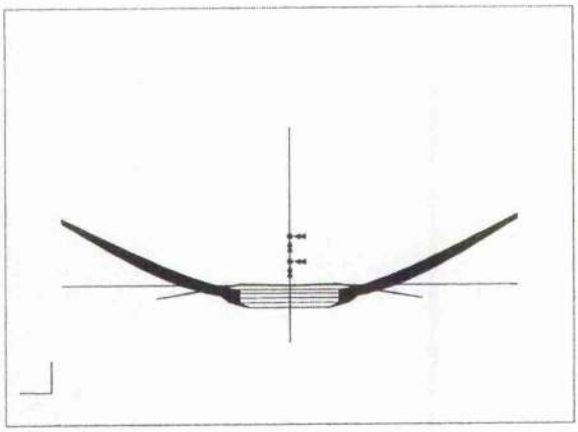

(c) Wing Symmetric

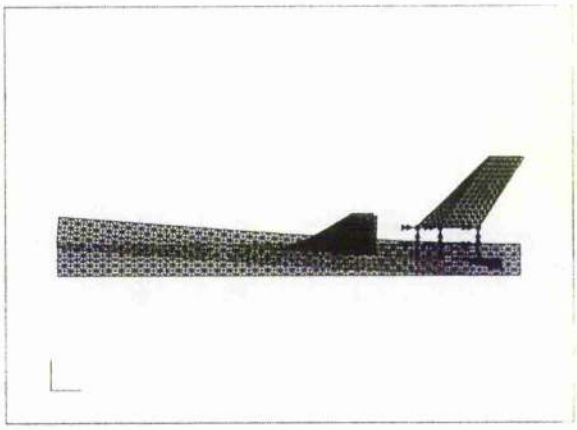

(d) Fuselage Vertical Bending

Figure 3.6: Modes for Structural Model 2

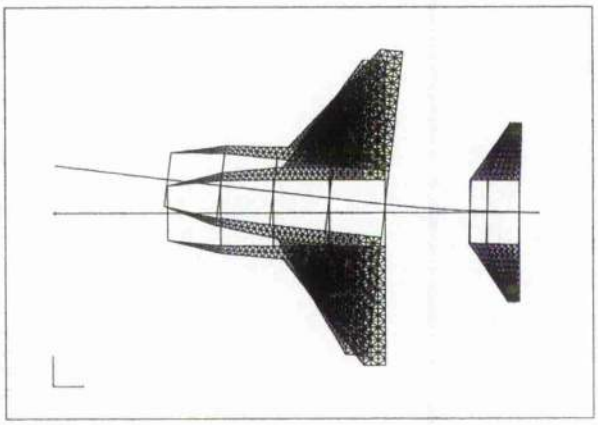

(a) Fuselage Lateral Bending

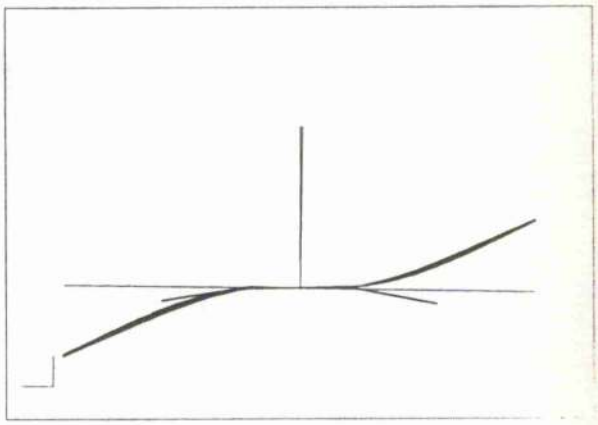

(b) Wing Antisymmetric

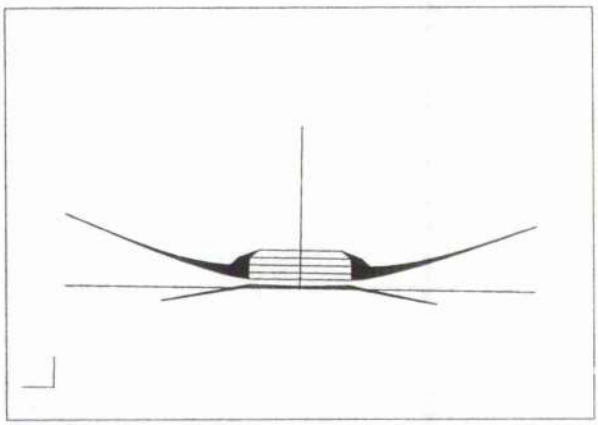

(c) Wing Symmetric

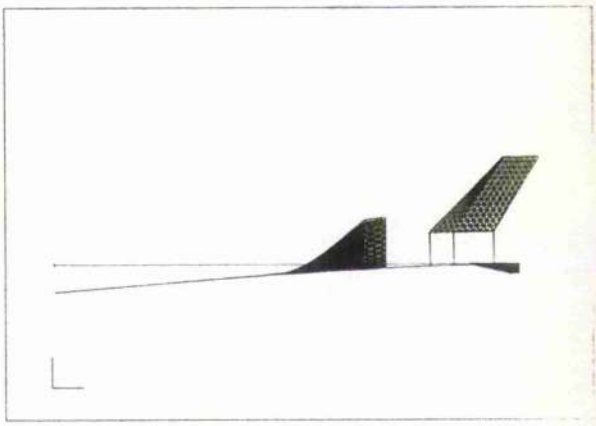

(d) Fuselage Vertical Bending

Figure 3.7: Modes for Structural Model 3

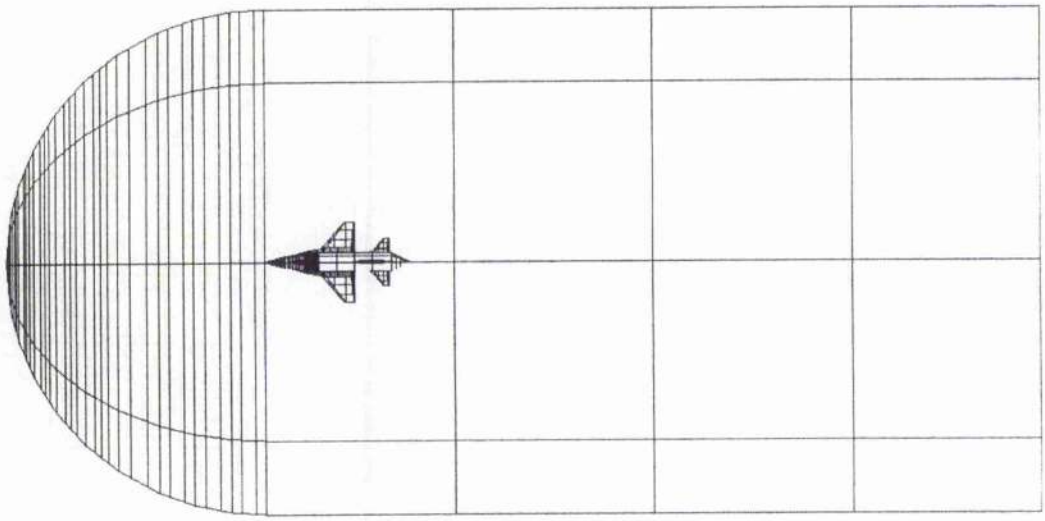

Figure 3.8: The aircraft and it's farfield flow boundaries

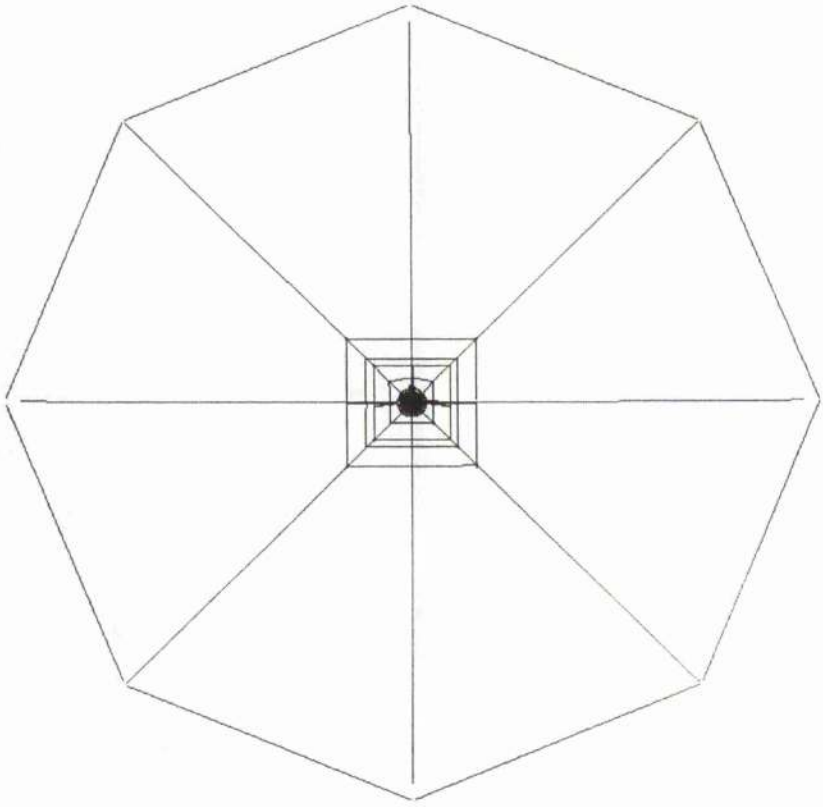

Figure 3.9: The O-Grid blocking

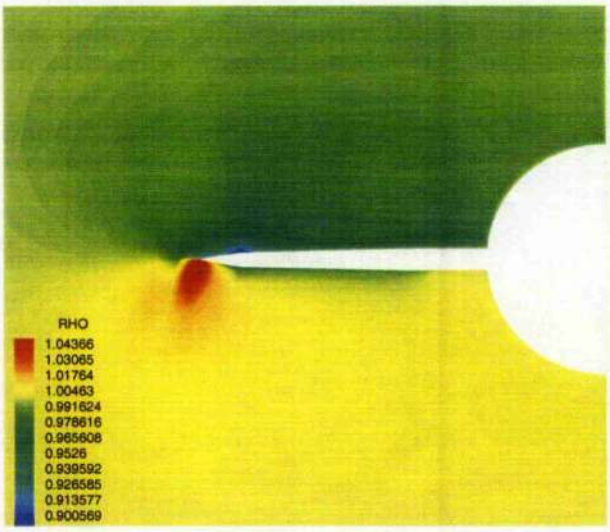

(a) Section through the plane x/c=2.5

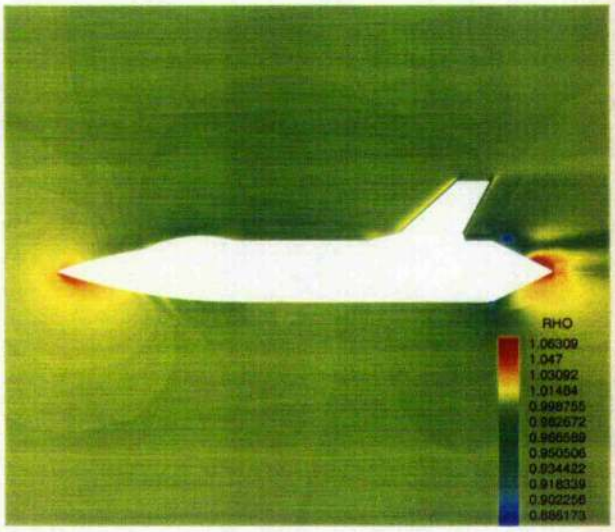

(b) Section through the plane z/c=0

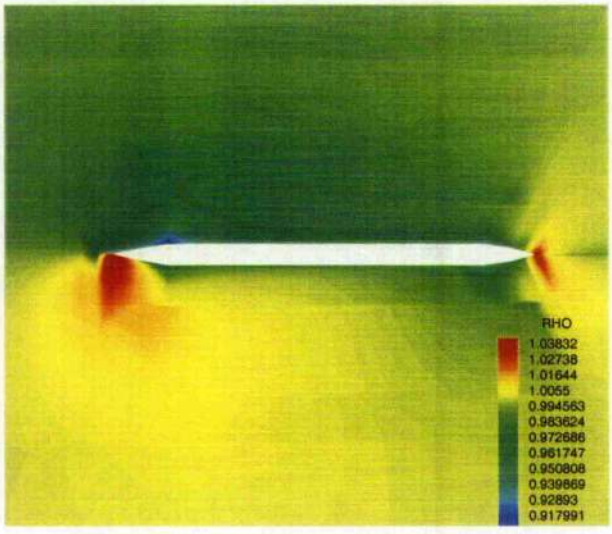

(c) Flow over wing section through the plane z/c=0.5

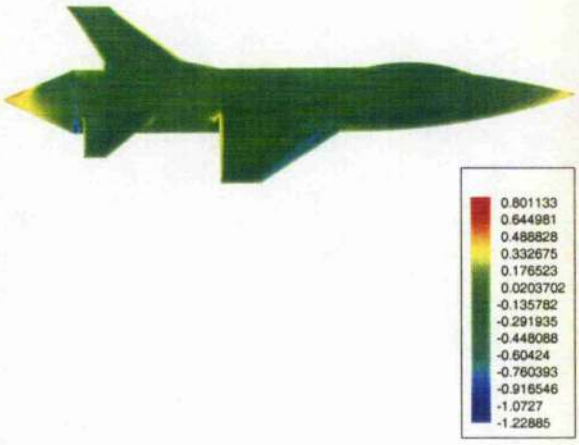

(d) Cp contours on the surface

Figure 3.10: Density and Cp contours on the coarse grid at Mach 0.5 and angle of attack 5°

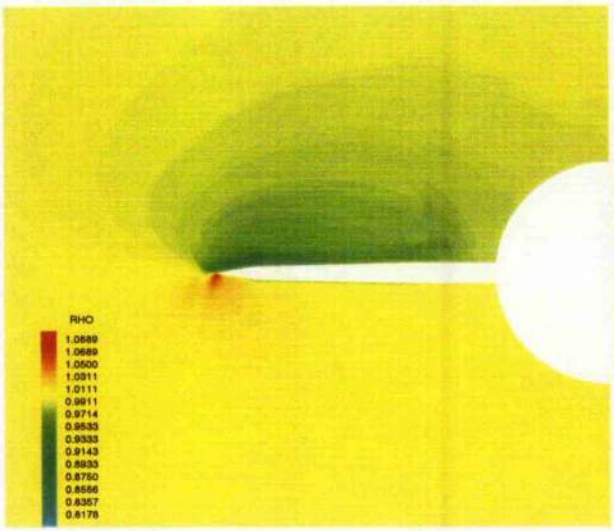

(a) Section through the plane x/c=2.5

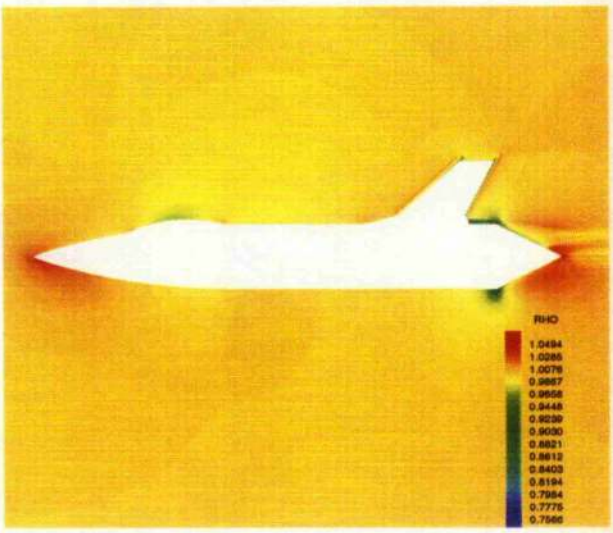

(b) Section through the plane z/c=0

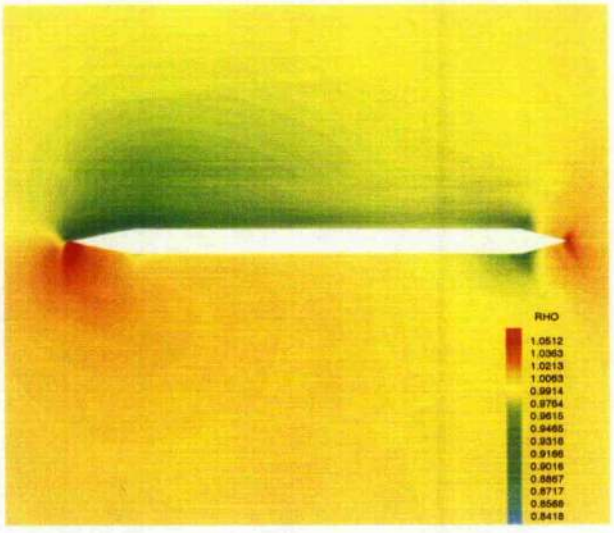

(c) Flow over wing section through the plane z/c=0.5

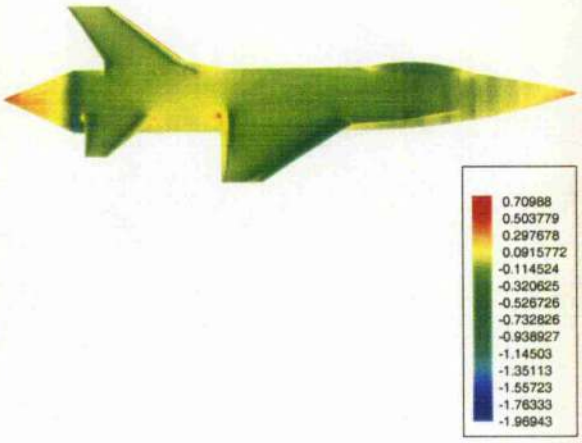

(d) Cp contours on the surface

Figure 3.11: Density and Cp contours on the fine grid at Mach 0.5 and angle of attack 5°

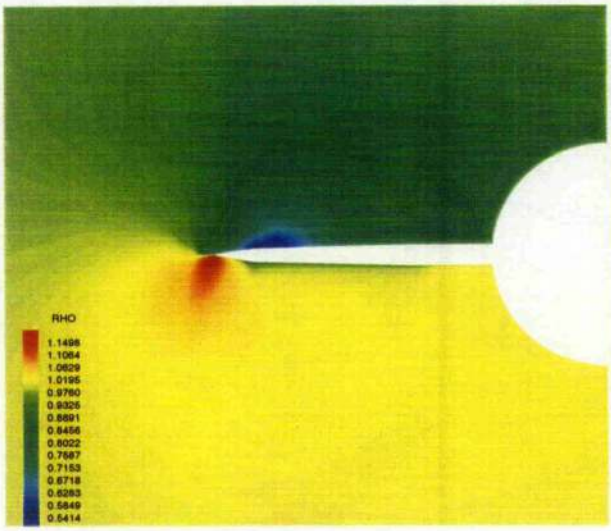

(a) Section through the plane x/c=2.5

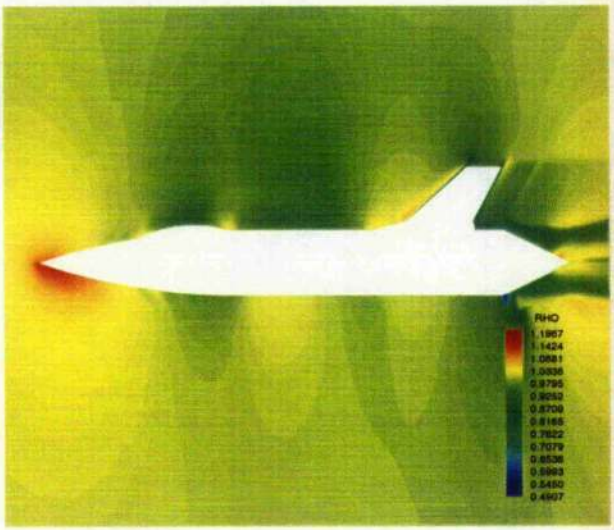

(b) Section through the plane z/c=0

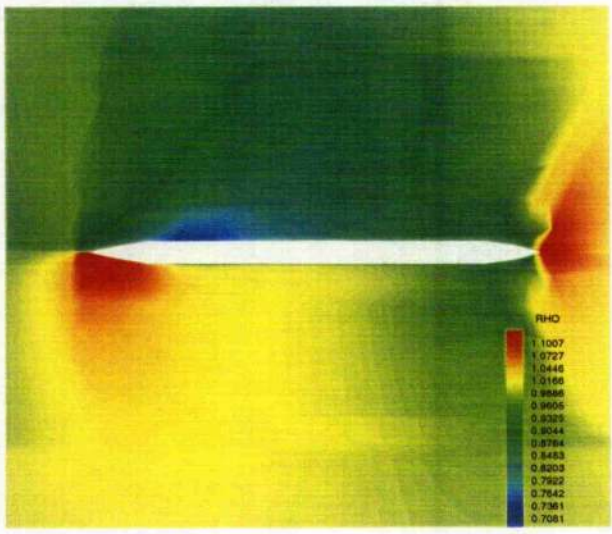

(c) Flow over wing section through the plane z/c=0.5

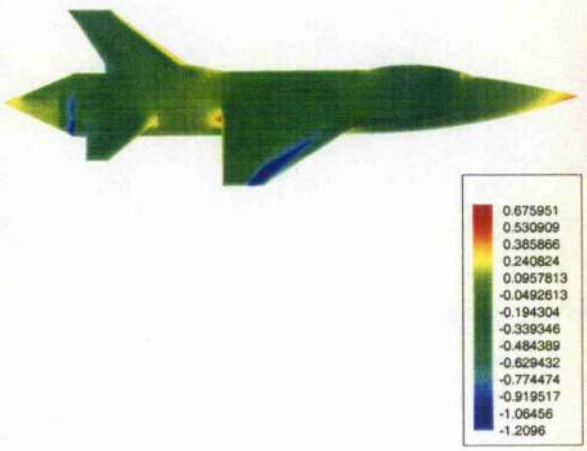

(d) Cp contours on the surface

Figure 3.12: Density and Cp contours on the coarse grid at Mach 0.9 and angle of attack 5°

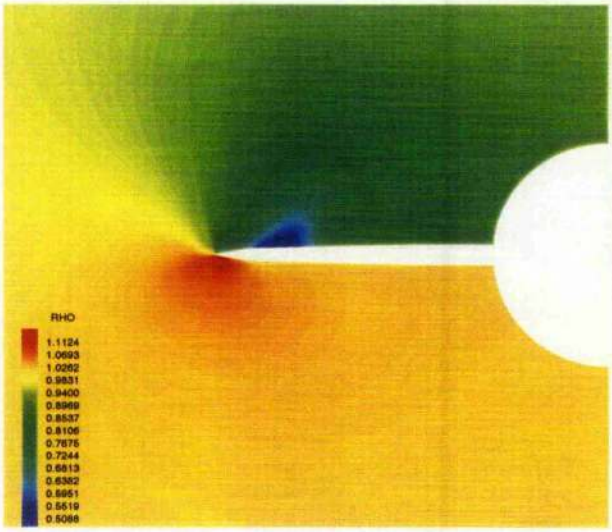

(a) Section through the plane x/c=2.5

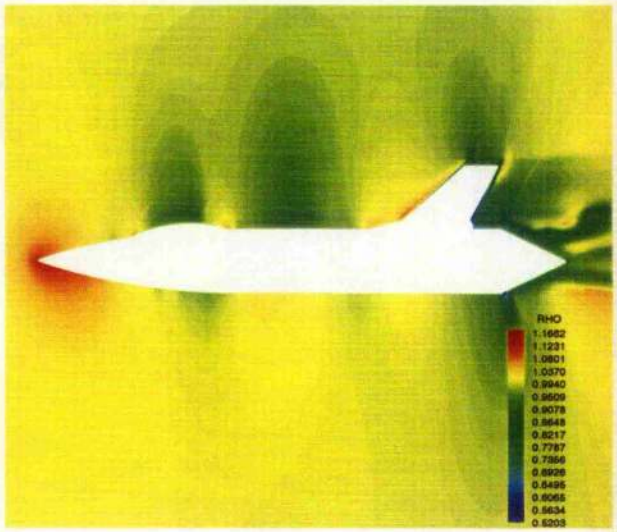

(b) Section through the plane z/c=0

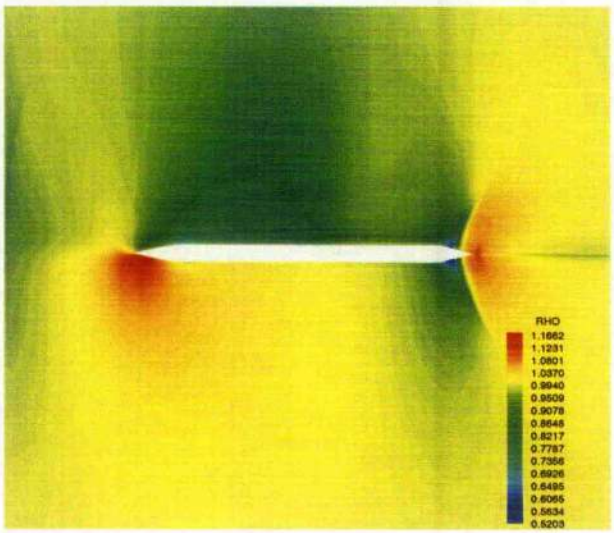

(c) Flow over wing section through the plane z/c=0.5

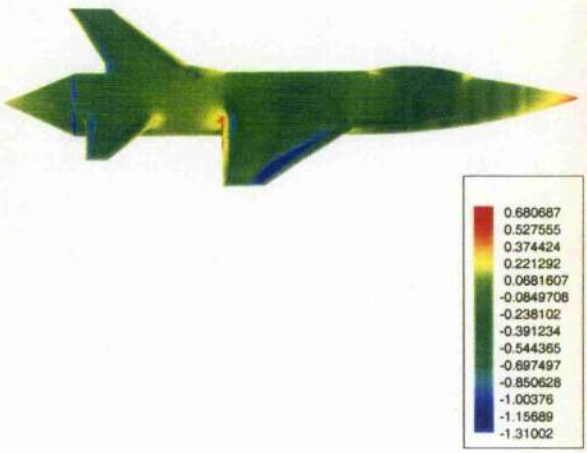

(d) Cp contours on the surface

Figure 3.13: Density and Cp contours on the fine grid at Mach 0.9 and angle of attack 5°

Chapter 4

Transformation Methodology

Accurate transformation of deformation and load data between the structural and fluid grids is of great importance for the correct prediction of flutter boundaries. Good FEM and CFD solvers will not give accurate aeroelastic results if the transformation scheme linking them is inaccurate. Development and application of a good transformation scheme for a fighter aircraft forms the main objective of the current thesis. As described in Chapter 3 the fuselage is simulated as a beam or a plate and the wings, horizontal stabilizer and the vertical fin as plates. Since the CVT technique can be applied only on 2 and 3 dimensional structural grids a new transformation scheme for the fuselage has been developed and applied to the current test case. Both of these transformation schemes are described in the following sections. A second issue is that of ensuring that the components match after transformation at the component interfaces.

4.1 Constant Volume Tetrahedron

The CVT scheme is a transformation technique proposed in [14]. A surface element consisting of the three nearest structural grid points $\mathbf{x}_{s,i}(t)$, $\mathbf{x}_{s,j}(t)$ and $\mathbf{x}_{s,k}(t)$ to a given fluid grid point $\mathbf{x}_{a,l}(t)$ is identified. Once the structural grid points are

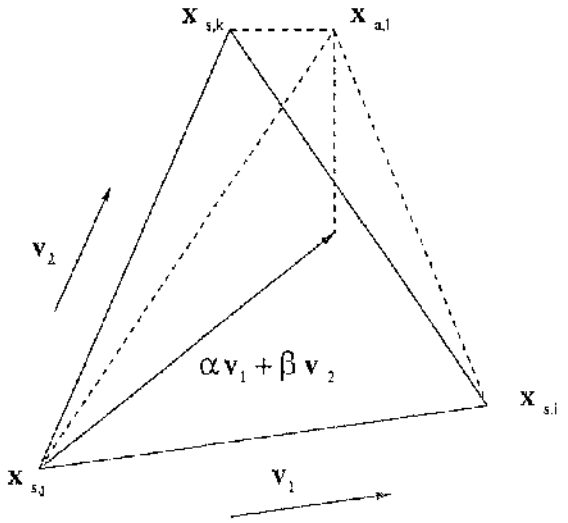

α

Figure 4.1: The Constant Volume Tetrahedron (from [14])

identified and associated with the fluid grid point the position of $\mathbf{x}_{a,l}$ is given by the expression

$$\mathbf{c} = \alpha\mathbf{a} + \beta\mathbf{b} + \gamma\mathbf{d} \tag{4.1}$$

where $\mathbf{a} = \mathbf{x}_{s,j} - \mathbf{x}_{s,i}, \mathbf{b} = \mathbf{x}_{s,k} - \mathbf{x}_{s,i}$, and $\mathbf{d} = \mathbf{a} \times \mathbf{b}$. From the above the constants $\alpha, \beta$and γ are calculated as

$$\alpha = \frac{|\mathbf{b}|^2(\mathbf{a}.\mathbf{c}) - (\mathbf{a}.\mathbf{b})(\mathbf{b}.\mathbf{c})}{|\mathbf{a}|^2|\mathbf{b}|^2 - (\mathbf{a}.\mathbf{b})(\mathbf{a}.\mathbf{b})} \tag{4.2}$$

$$\beta = \frac{|\mathbf{a}|^2(\mathbf{b}.\mathbf{c}) - (\mathbf{a}.\mathbf{b})(\mathbf{a}.\mathbf{c})}{|\mathbf{a}|^2|\mathbf{b}|^2 - (\mathbf{a}.\mathbf{b})(\mathbf{a}.\mathbf{b})} \tag{4.3}$$

$$\gamma = \frac{(\mathbf{c}.\mathbf{d})}{|\mathbf{d}|^2} \tag{4.4}$$

The position of the fluid grid point $\mathbf{x}_{a,l}$ is denoted by the sum of the in-plane component $\alpha\mathbf{a} + \beta\mathbf{b}$ and out of plane component $\gamma\mathbf{d}$ which is normal to the plane

of the structural points. The volume of the tetrahedron is given by

$$V = \frac{\mathbf{a}.(\mathbf{b} \times \mathbf{c})}{4} \tag{4.5}$$

As the volume of the tetrahedron remains constant the fluid grid position is given by

$$\mathbf{x}_{a,l} = \mathbf{x}_{s,i}(t) + \alpha \mathbf{a}(t) + \beta \mathbf{b}(t) + \gamma(t)\mathbf{d}(t) \tag{4.6}$$

with α and β fixed at their initial values and γ calculated as

$$\gamma(t) = \frac{|\mathbf{d}(0)|^2}{|\mathbf{d}(t)|^2}\gamma(0). \tag{4.7}$$

Equation (4.7) means that the projection of the fluid grid point on the structural element moves linearly with the structural element where the out of plane component is chosen to conserve the volume of the tetrahedron. If the fluid and the structural points are planar then the expression reduces to linear interpolation for the position of the fluid point. Equation (4.6) can be expressed in a linearised form as follows

$$\delta \mathbf{x}_{a,l} = \mathrm{A}\delta \mathbf{x}_{s,i} + \mathrm{B}\delta \mathbf{x}_{s,j} + \mathrm{C}\delta \mathbf{x}_{s,k} \tag{4.8}$$

$$\begin{aligned} \mathrm{A} &= \mathrm{I} - \mathrm{B} - \mathrm{C} \\ \mathrm{B} &= \alpha \mathrm{I} - \gamma \mathcal{U}\mathcal{V}(\mathbf{b}) \\ \mathrm{C} &= \beta \mathrm{I} + \gamma \mathcal{U}\mathcal{V}(\mathbf{a}) \\ \mathcal{U} &= \mathrm{I} - \frac{2}{|\mathbf{d}|^2}\mathcal{D}(\mathbf{d})\mathcal{S}(\mathbf{d}) \end{aligned} \tag{4.9}$$

$$\mathcal{V}(\mathbf{z}) = \begin{pmatrix} 0 & -z_3 & z_2 \\ z_3 & 0 & -z_1 \\ -z_2 & z_1 & 0 \end{pmatrix} \tag{4.10}$$

$$\mathcal{D}(\mathbf{z}) = \begin{pmatrix} z_1 & 0 & 0 \\ 0 & z_2 & 0 \\ 0 & 0 & z_3 \end{pmatrix} \tag{4.11}$$

$$\mathcal{S}(\mathbf{z}) = \begin{pmatrix} z_1 & z_2 & z_3 \\ z_1 & z_2 & z_3 \\ z_1 & z_2 & z_3 \end{pmatrix} \tag{4.12}$$

To minimize the error of the linearised CVT the linearisation is updated at the latest fluid and surface grid positions i.e. after each update of the structural position during aeroelastic calculations. Hence the values of **a**, **b**, and **c** are calculated at the latest grid positions. In the linearised CVT used for the current work α and β are calculated as follows.

It was found in [14] that the linearisation error introduced can significantly effect the static and dynamic responses computed. Therefore, the matrices **A**, **B** and **C** are updated every time the surface is moved so that the linearisation can be considered as being about the latest fluid and structural positions. The values of the transformed deflections have to be interpreted accordingly. This method is found to give geometrically identical results to using the full nonlinear method. The cost of computing the matrices is very small compared to the flow solution itself.

4.2 1D Constant Volume Tetrahedron

For structural components modelled as 1 dimensional beams (eg. the fuselage in this work) the CVT transformation does not work without some modification. In the original CVT, to form a tetrahedron 3 structural points forming a triangle are required. For an undeformed 1D beam element this is not possible as the structural

points do not form a plane. One possible solution would be to create a structural triangle by adding in a fictitious point close to one of the structural nodes so that the two nodes of the beam element along with the fictitious point forms a triangular element. When the structure deforms the displacement of this fictitious point is calculated as equal to the displacement of the real structural point closest to it i.e. it undergoes only translation without adjusting the relative position to the bending of the fuselage. In the current work the method described above has been used for transformation of the fuselage for Structural Model 3. A fictitious third point for the structural grid was introduced for each 1D beam element. This point had the same x and z coordinates as one of the two points forming the 1D element. The y coordinate of the fictitious point has a unit more than that of the original point. Figure (4.2) shows the 1D structural element formed by the points $\mathbf{x}_{s,j}$, $\mathbf{x}_{s,i}$ and the fictitious structural point $\mathbf{x}_{s,k}$.

$$\mathbf{x}_{s,k} = \mathbf{x}_{s,i} + \hat{\mathbf{j}} \tag{4.13}$$

where $\hat{\mathbf{j}}$ is a unit vector in the direction of the y-axis. The triangular element formed is then used in the conventional CVT technique as described in section 4.1. This technique gives pure translation to the fluid points . No rotation is introduced, consistent with the motion of the points on the beam (refer Figure (4.3)). Consider the deformation of the node $\mathbf{x}_{s,i}$ which can be written as

$$\mathbf{x}^1_{s,i} = \mathbf{x}^0_{s,i} + \delta\mathbf{x}_{s,i} \tag{4.14}$$

where the superscript 1 and 0 represent the deformed and undeformed states of the structural nodes. The deformed fictitious node can then be calculated as

$$\mathbf{x}^1_{s,k} = \mathbf{x}^0_{s,k} + \delta\mathbf{x}_{s,i} \tag{4.15}$$

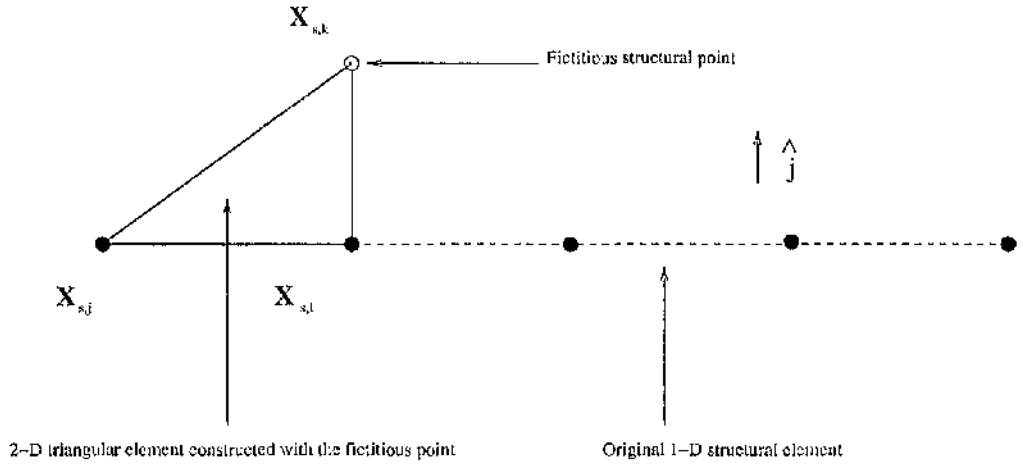

Figure 4.2: The 1D CVT fictitious point

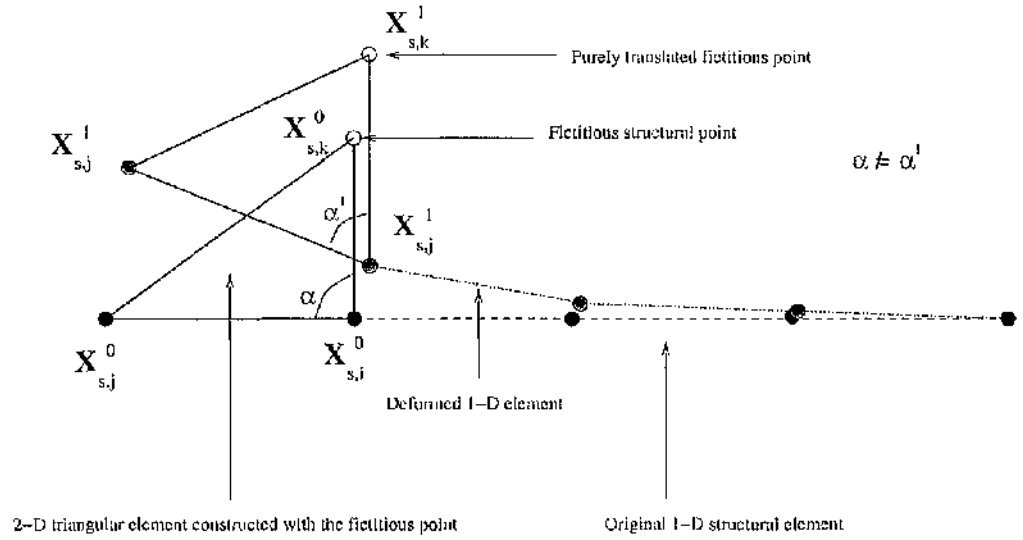

Figure 4.3: Translation of the 1D CVT element

4.3 Matching of Components

An aircraft is assembled from individual components. Hence deformation of the aircraft will include deformation of individual components in different planes. If the structural model has both 1D and 2D modelled components two different transformation schemes will be needed. These different transformation schemes might have considerable differences in their ability to transfer deformation information. Such a difference could spoil the grid smoothness around the boundary between regions of aerodynamic points transformed by different methods. This can be controlled in principle by

- Tuning the structural model
- Application of weighting scheme on the fluid nodes

These two methods are explained in the following sections.

4.4 Tuning the structural Model

An optimal structural model in terms of simplified geometry and ease of construction would provide the desired mode shapes having realistic frequencies and with properties allowing easy transformation of fluid surfaces. The structural model components should be able to adequately drive the deformation of the correct surfaces of the fluid surface grid. To achieve this the practices described in this section have been followed.

The component (wings, stabilizer and vertical fin) root is attached to the fuselage by a number of connectors. During FEM analysis the connectors serve the purpose of forcing the wings to have modal deformation that make the component root follow the fuselage deformation. This is important since, if the root section were not to

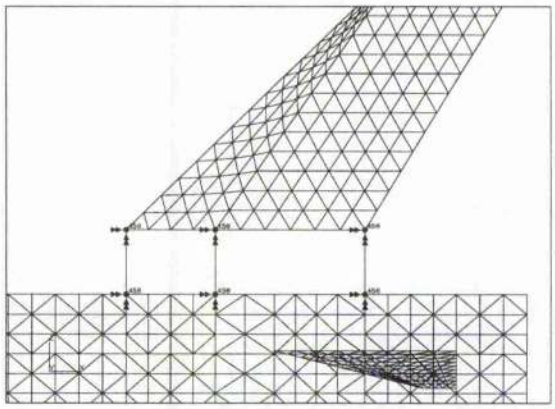

Figure 4.4: The rotational constraint condition on Structural Model 2

follow the fuselage deformation (due to lack of adequate connectors), there would be a wide difference in the deformation of the fuselage and the component root section. Additionally the connectors themselves have natural vibration which could bring about inconsistencies between the deformation of the fuselage and the root. This is overcome by giving rotational constraints to the connectors. In Structural Models 1, 2 and 3 the vertical fin root is prevented from twisting by giving the connectors a boundary condition restricting their rotation i.e. the two nodes of the connectors do not have movement relative to each other (refer Figure 4.4). The component then translates with the fuselage and the component root does not move relative to the fuselage. For higher modes of vibration there is usually an amount of twisting of the components with respect to the fuselage, by applying the constraints this can be avoided at the component roots and hence a grid smoothness at the interface is promoted.

4.5 Weighting Scheme

A version of the CVT is required which can do the transformation for the complete aircraft with the minimum of manual intervention and which preserves the surface mesh, particularly at junctions between components. The insight for the method

is provided by the paper of Melville [28] which treats the aircraft components in a hierarchy.

The first stage of the method is to partition the fluid and structural points into levels associated with components. The primary component is the fuselage since all the other parts of the aircraft are connected to it. The fluid and structural grid points on the fuselage are therefore designated as being of level 1. Next, the wings, horizontal stabilizer and the vertical fin are connected to the fuselage and the fluid and structural grid points on these components and the fuselage are designated level 2. The idea of the hierarchy is that level 2 points have a primary motion due to the fact that they are connected to the fuselage and a secondary motion due to their own elasticity. Extra components attached to the wing, such as fuel tanks and stores would be designated level 3, with their primary motion being due to the fact that they are attached to the wing.

At this stage a number of subsets of points have been defined for the fluid and structural grids, with one subset for each level. Denote the set of aerodynamic points in level m as $\mathcal{A}^m$ and the structural points as $\mathcal{S}^m$. The lowest level (2 in this case) contains all of the points in the respective grids and level $m+1$ is a subset of level m.

The first stage for the CVT as described above is to associate each fluid point with three structural points. This is done in practice by defining a triangularisation of the structural grid and then searching for the nearest centroid to each aerodynamic point. This mapping can be done over the structural points in each level as well, defining level one and two mappings. In the current case the level one mapping will have all points in the fluid grid driven only by points on the fuselage. The level two mapping is equivalent to the original CVT method applied to all grid points without restriction. The transformation of the 4th mode in structural model 3 (see Figure 3.7(d)) is shown in Figure (4.11 and 4.12) using successively the first and second level mappings. The first level mapping leads to the fluid motion following the

fuselage, with the wings being moved in a rigid fashion. The second level mapping introduces the wing bending as well, with the motion of the fuselage being identical to that arising from the first level mapping.

A problem with the level two mapping arises at junctions between components. This is illustrated in Figures (4.5)-(4.7). A second problem arises where the fin is attached to the fuselage, as shown in Figures (4.8)-(4.10). For the level two mapping the nodes that are not on the fuselage are being driven by a different transformation from those actually on the junction, which are driven by the fuselage. This leads to a small but disastrous distortion of the grid in the junction regions. Using the level one mapping treats all points in a consistent way and maintains the grid quality in the junction regions as a result. However, the level one mapping misses all effects introduced by the elasticity of the non-fuselage components, since these structural components are not used to drive the fluid surface grid. A new method is therefore needed to correctly transform the complete deformation while avoiding the problems at junctions.

The basis for the method is the observation that the level one and two transformed mode shapes on level two components in regions close to the fuselage are almost identical. This follows from the observation of Melville [28] that the fuselage drives the wing motions and this effect is dominant close to the wing root as opposed to any wing alone elastic effects. The method therefore blends the level one and two transformed fluid points, giving priority to the level one transformation as we approach the fuselage (in general the level m transformation is given priority as the level m component is approached). This means that in the junction region the fluid grid is transformed from the fuselage structural model rather than the wing.

Denote the transformed deflection for a fluid point $\mathbf{x}_{a,l}$ using the mth level mapping as $\delta\mathbf{x}^m_{a,l}$. The blending used to give the final transformed displacement is given as

$$\delta\mathbf{x}_{a,l} = \Sigma_{m=1}^{n} w_{m,l}\delta\mathbf{x}^m_a. \tag{4.16}$$

The weights for the blending $w_{m,l}$ must add to one. To define the values of the weights for level m we need to consider the distance from the components associated with that level. Define the nearest distance of the point $\mathbf{x}_{a,l}$ to all of the points in level m by $d_{m,l}$. It is a simple matter to calculate $d_{m,l}$ by searching over the fluid points defined in level m for the nearest point. If $\mathbf{x}_{a,l}$ actually belongs to level m then $d_{m,l} = 0$. Then, the weights for blending the two levels of transformation in the current test case are computed from

$$w_{1,l} = e^{-10 d_{m,l}} \tag{4.17}$$

and

$$w_{2,l} = 1 - w_{1,l}. \tag{4.18}$$

For points on the fuselage the entire weight will be put on the fuselage driven transformation, for points close to the fuselage most weight will be given to the fuselage driven transformation and otherwise most weight is given to the level two component driven transformation. The exponential function was found to be suitable for the current test case but some experimentation with functions for other cases may be required. The comparison between the transformed fourth mode using the blended transformation and the level two transformation is shown in Figure (4.13 and 4.14) indicating that there is little difference between the two. However, looking to the junction region, the blended transformation has avoided the folded grid as required. Also, the fin now remains cleanly attached to the fuselage as opposed to the level two transformation. Since the cost of computing the original CVT transformation is small, the cost of applying the new multi-level scheme is also small. On cost grounds there is an objection to using the exponential function in the weighting but the weights are calculated as part of a preprocessing step so this is insignificant.

4.6 Results

The two level transformation was applied on the three Structural Models described in the previous chapter and the transformed mode shapes were checked for any irregularities in the surface grid smoothness that may cause problems during the time marching aeroelastic calculations. There was no undesirable roughness in the transformed aircraft surface grid found. The two level transformation results for the first four modes of Structural Model 3 are given in Figure (4.15).

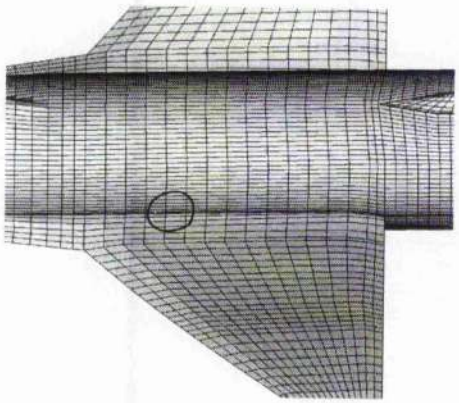

Figure 4.5: The fuselage wing interface. Circle indicates area of interest

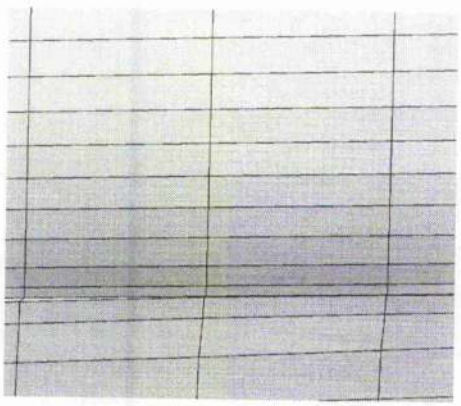

Figure 4.6: Fuselage wing interface using one level transformation

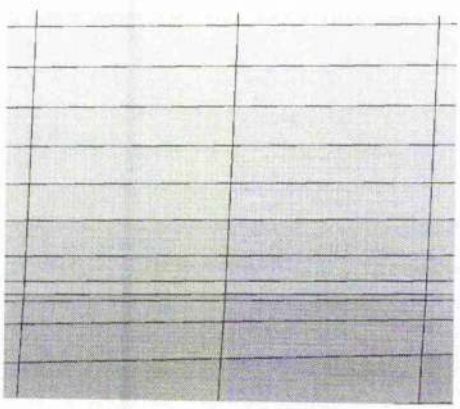

Figure 4.7: Fuselage wing interface using two level transformation

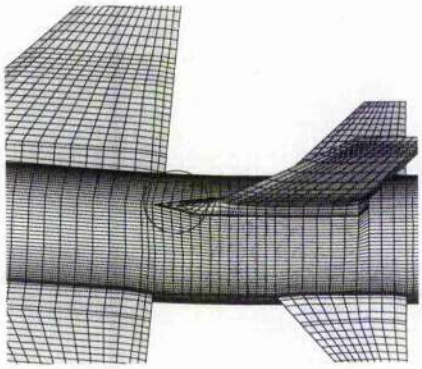

Figure 4.8: The fuselage vrtical fin interface. Circle indicates area of interest

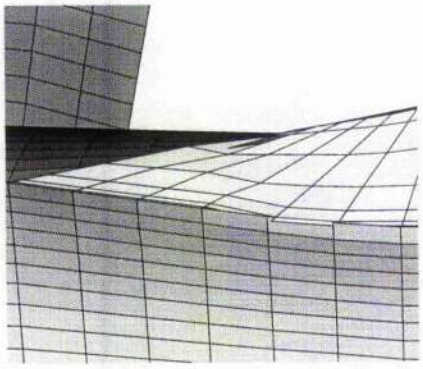

Figure 4.9: Fuselage vertical fin interface using one level transformation

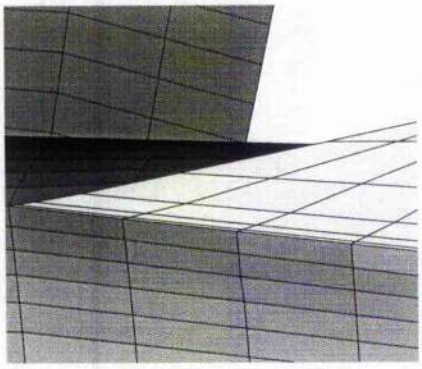

Figure 4.10: Fuselage vertical fin interface using two level transformation

Figure 4.11: The level 1 transformation for the 4th mode

Figure 4.12: The blended transformation for the 4th mode

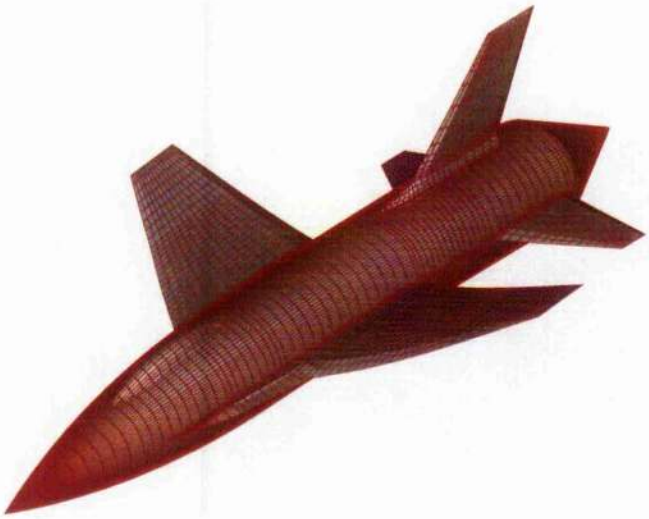

Figure 4.13: The blended transformation for the 4th mode

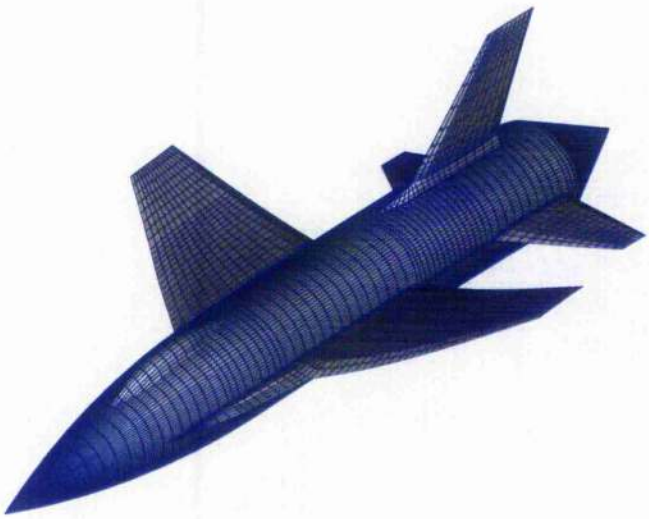

Figure 4.14: The level 2 transformation for the 4th mode

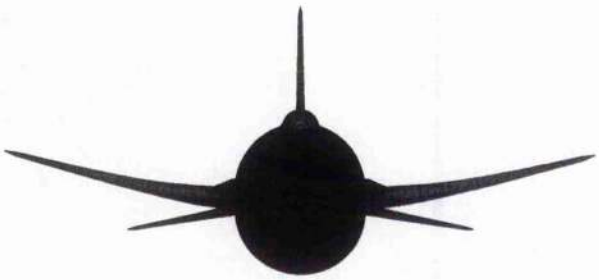

(a) Wing Symmetric

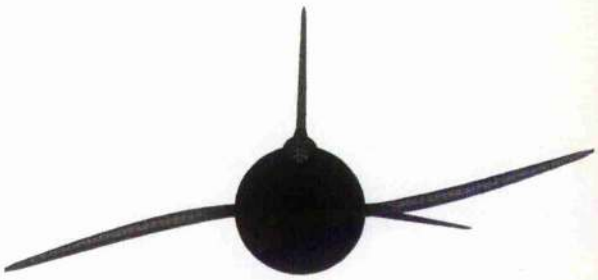

(b) Wing Antisymmetric

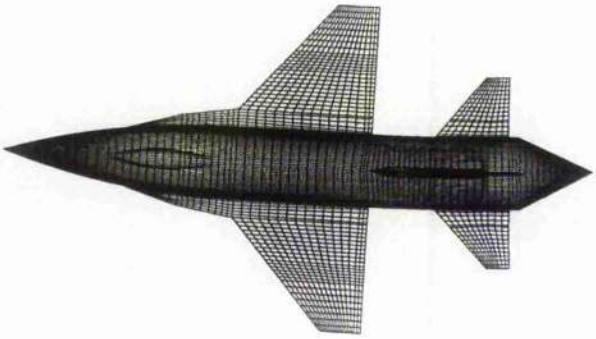

(c) Fuselage Lateral Bending

(d) Fuselage Vertical Bending

Figure 4.15: Transformed mode shapes of Structural Model 3 (see Figure (3.7))

Chapter 5

Conclusion

5.1 Results

A successful transformation methodology for a complete aircraft configuration was developed and applied. A 1D CVT technique was developed for beam structures and seamlessly combined with the original CVT to carry out transformation on aircraft structural models having both 1D and 2D components. A two level weighting methodology was developed and successfully applied with the transformation technique to give accurate transformed fluid surface grids without any damage to the grids at component interfaces. A number of cases were studied for the effect of fuselage twist on the transformation and the ability of the weighting scheme to handle this. The CFD blocking and grid constructed for the aircraft can be used for future proposed aeroelastic work

5.2 Future Work

In this project a CFD volume grid has been built, a transformation scheme for complete aircraft has been developed, and structural models that are suitable for flutter analysis, subject to minor modifications, have been constructed. The next step will

be to carry out time marching flutter calculations on the complete aircraft using the above. An immediate requirement before this can be done is the development of an improved fluid grid deformation technique. The existing technique deforms the grid only in the block containing the aircraft surface grid. For large aircraft deformation the blocks themselves have to adjust positions. Such an algorithm for parallel CFD codes has been published in the literature [37] and needs to be incorporated in PMB3D. The time marching flutter analysis results thus obtained can be then be compared with the flutter results from commercial linear codes. Interesting conclusions could be drawn from the comparison with respect to the influence of aerodynamic nonlinearities on the computed aeroelastic results.

The thesis has examined one aspect of constructing a CFD based flutter simulation. Some of the more advanced topics like control surface flutter add additional complexity which can now be considered. Prediction of control surface loads is an important issue for improving aircraft performance and stability. An accurate numerical simulation of this in the transonic flow regime would require an Euler/Navier-Stokes based flow solver, like PMB3D, to take into account the flow nonlinearities in such a regime. Also a method for modelling the control surface deformation would be needed. When a control surface is deflected it results in the modification of the geometry of the wing surface. This causes discontinuities along the control surface edges and the wing surface. A sliding grid method is currently being implemented in the code to deal with the control surface delfection. In this approach when the control surface is deflected the block containing the control surface slides with respect to the adjacent blocks. The approach that is being currently used is to blend the edges of the deflected control surface into the wing. Deformation of the grid in the block containing the deflected control surface is possible due to the blended edges.

With the insight and experience gained from the current work the groundwork has been laid for aeroelastic simulation on real aircraft geometries. A current project

involves aeroelastic analysis of the Hawk aircraft. The component fuselage interface of the structural model supplied for this aircraft does not make use of the connectors at the component roots. This will challenge the ability of the weighting scheme to deal with the inconsistencies at the junctions of the component fluid surface grid patches. Some of the structural models have most of the structural components modelled as 1D beam and are called "stick models". The new 1D CVT will be tested for these models.

The grid treatment for flaps described earlier will be used to to carry out control surface effectiveness studies for a free to roll aircraft/delta-wing. A successful simulation will enable to undertake optimisation studies on the size, shape and placement of the control surfaces on the wing.

An extension of the free to roll aircraft would be a fully deforming aircraft configuration. Such a test case would simulate aeroelasticity of a real aircraft with control surface deflected. The mode shapes for the structural grid could be obtained as in the current work, the deflection of the control surfaces could be performed as explained earlier and finally a three level weighting scheme would ensure the matching of the component interfaces. An extension from 2 level to 3 level weighting can easily be carried out for an aircraft with stores and flaps/ailerons/tabs. In the first level all the components would be mapped by the fuselage deformation. In the second level the major components like wings and tail fin would map the respective components and in the third and final level the control surfaces would be mapped by the respective deformed structural control surface grids (see section 4.5).

Once time marching flutter analysis yields realistic results store induced LCOs could be simulated. LCOs are thought to occur due to nonlinearities of the flow and structure. Amplitudes of oscillation grow exponentially for speeds beyond the flutter point. However the amplitudes do not grow to infinity but settle down to a constant value. This is because as the amplitude grow so does the nonlinear stiffness of the structure. Hence a point is reached when the energy transfer from the air can

no longer produce an exponential growth of oscillations.

One of the likely projects that could be considered include simulation of fuselage roll and tail loading due to the antisymmetric modes of the aircraft. This occurs due to twisting of the horizontal stabilizer during the wing antisymmetric mode of vibration. Further details from experiment/flight tests and from similar computational work are awaited for understanding of the problem before further progress could be made.

Bibliography

[1] E. F. Sheta et al. Computational and experimental investigation of limit cycle oscillations of nonlinear aeroelastic systems. *Journal of Aircraft*, 39(1):133–141, 2002.

[2] A. G. von Baumhauer and C. Koning, editors. On the Stability of Oscillations of an Airplane Wing, International Air Congress, London, United Kingdom, 1923.

[3] F. W. Lanchester. Torsional vibrations of the tail of an aeroplane. *R & M*, Part 1:276, 1916.

[4] W. H. Reed E. I. Garrick. Historical development of aircraft flutter. *Journal of Aircraft*, pages 898–912, 1981.

[5] R. A. Frazer and W. J. Duncan. The flutter of aeroplane wings. *Aeronautical Research Committee R & M*, 1155, 1928.

[6] B. von Schlippe. Zur frage der selbsterregten flügelschagungen. *Luftfahrforschung*, 13, February 1936.

[7] *Aviation Week*, December 1997.

[8] B. Donald. Wind tunnels of NASA. Technical Report SP:440, NASA, 1981.

[9] P. Garrison. Aircraft flutter. *Air & Space*, February, 2001.

[10] S. Pines, editor. An Elementary Explanation of the Flutter Mechanism. National Specialist Meeting on Dynamics and Aeroelasticity, Forth Worth-Texas. 1958. Institute of the Aeronautical Sciences.

[11] E. H. Dowell, editor. A Modern Course in Aeroelasticity. Kluwer Academic Press, 1995.

[12] I. W. Kaynes. Aeroelasticity review. Technical Report DERA/MSS/MSTR2/CR010456, DERA, February 2001.

[13] P. Geuzaine C. Farhat and G. Brown. Application of three field nonlinear fluid-structure formulation to the prediction of the aeroelastic parameters of an F-16 fighter. *Computers and Fluids*, 32:3 29, 2003.

[14] G. S. L. Goura. Time Marching Analysis of Flutter Using Computational Fluid Dynamics. PhD thesis, University of Glasgow, 2001.

[15] J. J. Meijer, B. J. G Eussen, M. H. L Hounjet et al. Perspectives of NLR aeroelastic methods to predict wing/store flutter and dynamic loads of fighter-type aircraft. Paper NLR-TP-2000-447, NLR.

[16] Y. F. Kao, D. D. Liu and K. Y. Fung. An efficient method for computing unsteady transonic aerodynamics of swept wings with control surfaces. *Journal of Aircraft*, 25(1):25–31, January 1988.

[17] D. M. Pitt and C. E. Goodman, editors. Flutter Calculations Using Doublet Lattice Aerodynamics Modified by Full Potential Equation, Proceedings of the 28th AIAA/ASME/ASCE/AHS Structures, Structural Dynamics and Materials Conference-AIAA-87-0882-CP, Monterey-California, 1987. AIAA.

[18] R. G. A. Silva and O. A. Fario Mello. Prediction of transonic flutter using Nastran with aerodynamic coefficients tuned to navier stokes computations.

Paper, Instituto de Aeronautica e Espa/ Centro Tecnico Aeroespacial, Sao Jose dos Campos - SP - Brazil.

[19] B. E. Richards K. J. Badcock and M. A. Woodgate. Elements of computational fluid dynamics on block structured grids using implicit solvers. *Progress in Aerospace Sciences*, 36:351–392, 2000.

[20] G. P. Guruswamy. A review of numerical fluids/structures interface methods for computations using high fidelity equations. *Computers and Structures*. 80(1):31–41, January 2002.

[21] G. P. Guruswamy. Unsteady aerodynamic and aeroelastic calculations of wings using euler equations. *AIAA Journal*, 28(3):461–469, 1990.

[22] Manoj K. Bhardwaj. A CFD/CSD Interaction Methodolgy for Aircraft Wings. PhD thesis, Virginia Polytechnic Institute and State University. 1997.

[23] C. J. Borland and D. P. Rizzetta. Nonlinear transonic flutter analysis. *AIAA Journal*, 20(11):1606–1615, 1982.

[24] J. T. Batina II. J. Cunningham and R. M. Bannett. Modern wing flutter analysis by computational fluid dynamic methods. *Journal of Aircraft*. 25(10):962 968, October 1988.

[25] J. Vadyak D. Schuster and E. Atta, editors. Static Aeroelastic Analysis of Fighter Aircraft Using a Three Dimensional Navier Stokes Algorithm. AIAA 903-0435, 1990.

[26] E. M. Lee-Rausch and J. T. Batina. editors. Calculation of Agard Wing 445.6 Flutter Using Navier-Stokes Aerodynamics. AIAA Applied Aerodynamics Conference-AIAA-93-3476-CP, Monterey-California, 1993. AIAA.

[27] G. P. Guruswamy and C. Byun. Direct coupling of euler flow equations with plate finite element structures. *AIAA Journal*. 33(2):375–377, 1994.

[28] R. Melville, editor. Nonlinear Simulation of Aeroelastic Instability. AIAA 2001-0570, 2001.

[29] M. Lesoinne C. Farhat and P. LeTallec. Load and motion transfer algorithm for fluid/structure interaction problems with non-matching discrete interfaces: Momentum and energy conservation, optimal discretization and application to aeroelasticity. *Computer Methods in Applied Mechanics and Engineering.* 157:95–114, 1998.

[30] R. L. Harder and R. N. Desmarais. Interpolation using surface splines. *Journal of Aircraft*, 9(2):189–191, February 1972.

[31] K. Appa. Finite-Surface spline. *Journal of Aircraft*, 26(5):495–496, 1989.

[32] K. J. Bathe. Finite Element Procedures in Engineering Analysis. Prentice Hall. 1982.

[33] V. Murti and S. Valliappan. Numerical inverse isoparametric mapping in remeshing and nodal quantity contouring. *Computers and Structures*, 22(6):1011–1021, 1986.

[34] P. C. Chen and I. Jadic. Interfacing fluid and structural models via innovative structural boundary element method. *AIAA Journal*, 36(2):282–287, February 1998.

[35] C. A. Brebbia and J. Dominguez. Boundary Elements: An Introductory Course. McGraw-Hill, 1992.

[36] X. Z. Huang and S. Zan. Wing and fin buffet on the standard dynamic model. RTO Report RTO-TR-26 AC/323(AVT)TP/19, IAR/NRC Canada. October 2000.

[37] H. M. Tsai et al. Unsteady flow calculations with a parallel mutiblock moving mesh algorithm. *AIAA Journal*, 39(6):1021 1029. June 2001.